Métodos computacionales en muografía de absorción

Universidad de los Andes | Facultad de Ciencias Departamento de Física

2026

Taller: Aplicaciones Interdisciplinarias de Detectores de Particulas

Junio 10 – 12.

MuTe The Muon Telescope

LIDeRA

Universidad Industrial de Santander

CYTED

LAGO

Rafael Martínez Rivero
Grupo de Investigación en Relatividad y Gravitación (GIRG)
Laboratorio de Investigación para la Detección de Radiación y Astropartículas (LiDERA)
Universidad Industrial de Santander. Bucaramanga Colombia

10 June, 2026 Bogotá

rafael2248058@correo.uis.edu.co

Cosmic-ray **AI** **B**ackpropagation and **R**ay-tracing with **I**ntegrated **A**ngular scattering for **L**ow-cost **E**mulation and **S**imulation

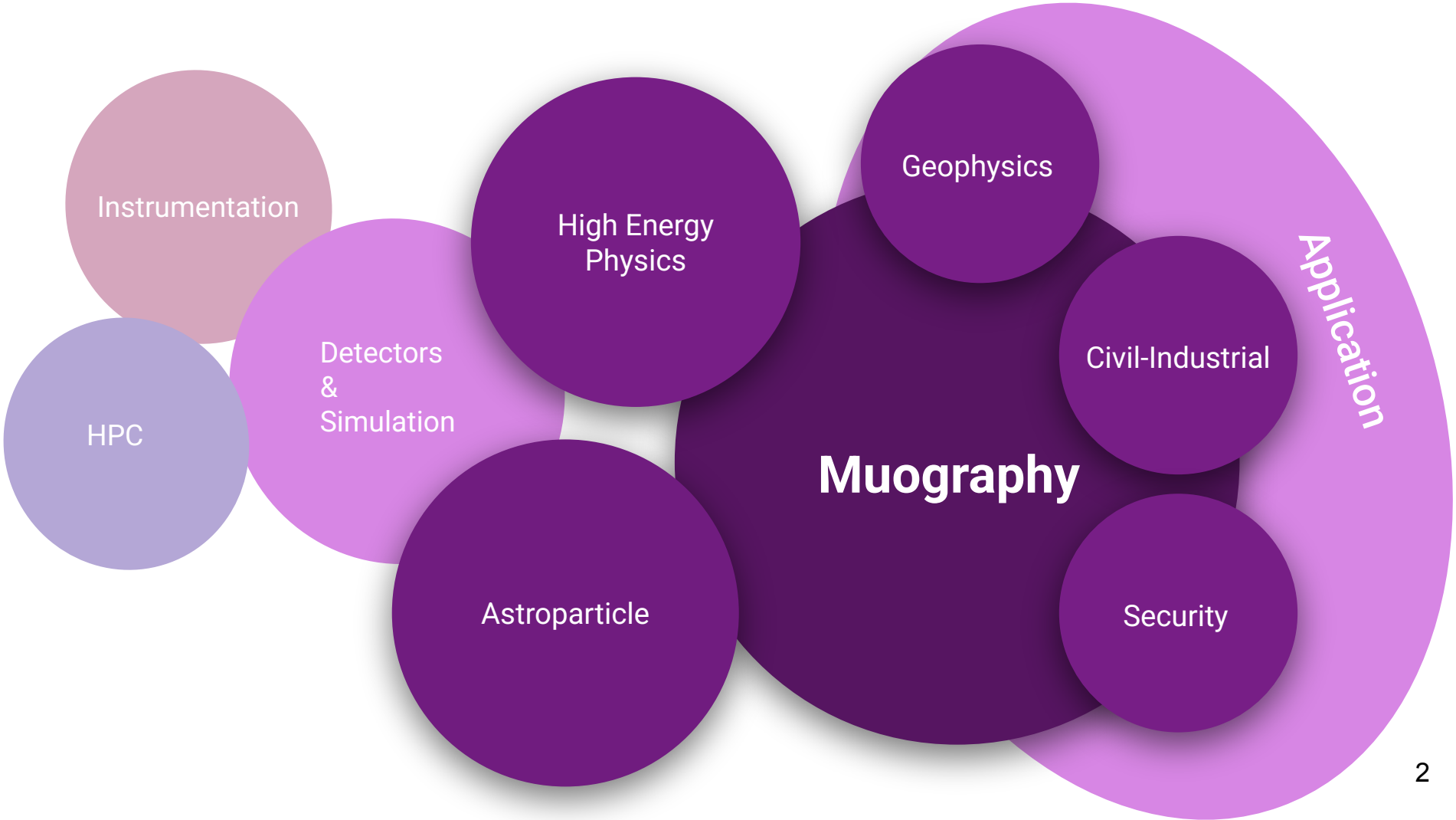
Instrumentation
HPC
Detectors
&
Simulation
High Energy
Physics
Astroparticle
Geophysics
Civil-Industrial
Security
Muography
Application

Muography on Mars and on the Moon

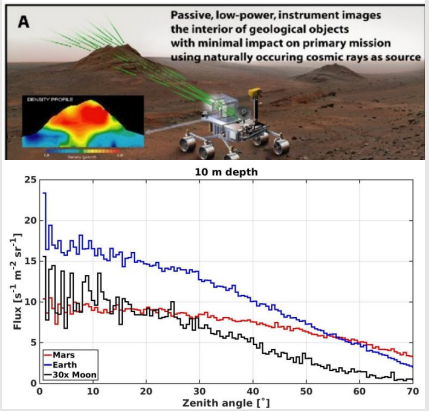

józsef Gábor Szűcs Muographers 2026-Talk

Exploring Hidden Cavities

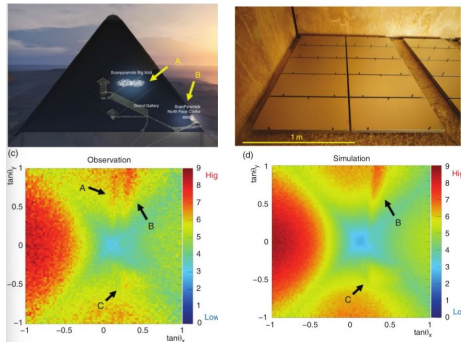

Morishima, K., et al. Nature 552, 386–390 (2017).
https://doi.org/10.1038/nature24647

Volcano Muography

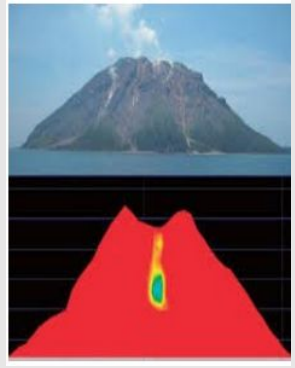

Oláh, L., Tanaka, H.K.M. (2025). Muography of Volcanoes.
https://doi.org/10.1007/978-3-031-86841-2_16

Undersea Muography

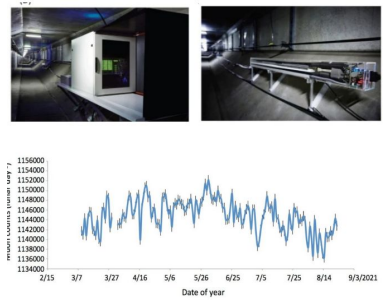

Tanaka,. *et al. Sci Rep* **12**, 6097 (2022).
https://doi.org/10.1038/s41598-022-10078-2

Muography of Tropical Cyclones

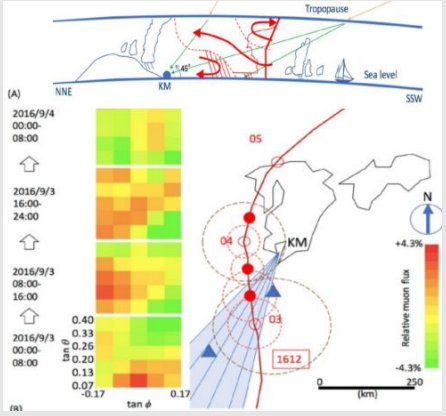

Tanaka et al. (2022) Sci. Rep. 12, 16710
https://doi.org/10.1038/s41598-022-20039-4

Inspection of Fukushima Daiichi Reactor

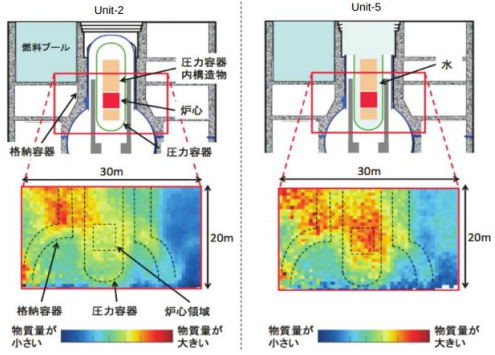

K. Morishima: Journal of the Photographic Society of Japan, 2016, Vol. 79, No. 1: 42-47

Detection of High-Z Materials

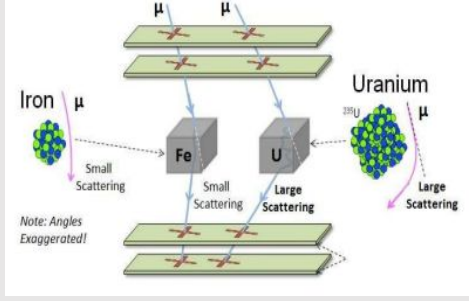

Pesente, S., et al.: NIM A 604, 738 (2009)
https://doi.org/10.1016/j.nima.2009.03.017

Muon Positioning (muPS)

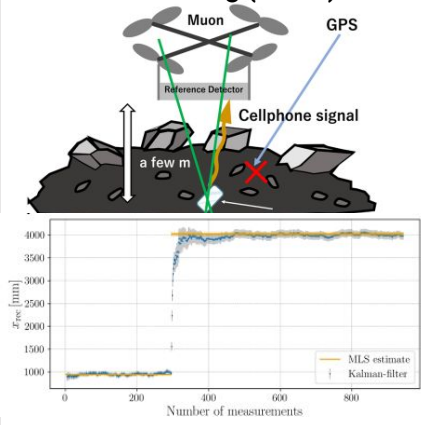

Varga, D., Tanaka, H.K.M. Sci Rep 14, 7605 (2024).
https://doi.org/10.1038/s41598-024-57857-7

Problema directo en muografia

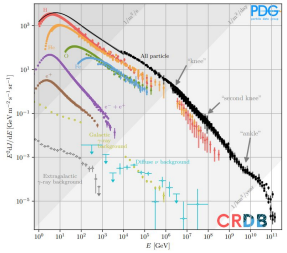

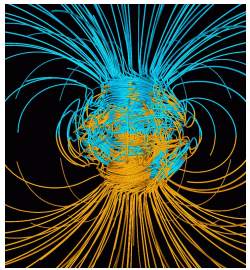

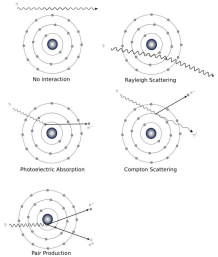

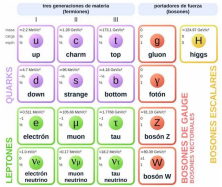

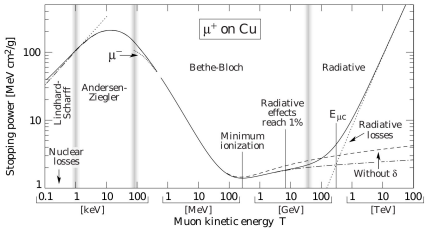

Astropartículas

Primarios, energías, composición química, campo geomagnético.

EAS/Flujo de entrada

Atmósfera, Interacciones UHECR, generación de secundarios.

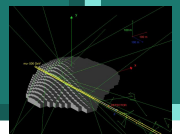

Objeto/Flujo de salida

Interacciones y transporte en la materia

Respuesta del detector

Geometría, Interacciones, eficiencias.

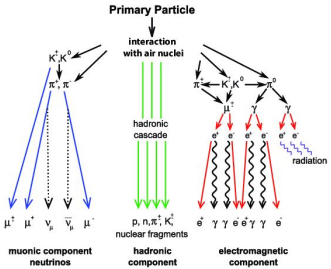

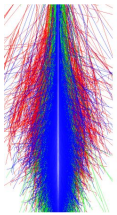

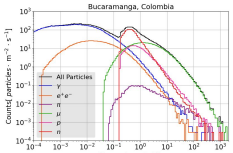

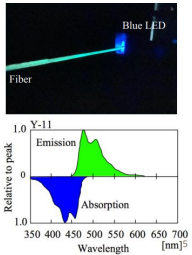

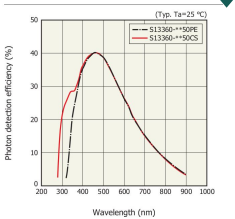

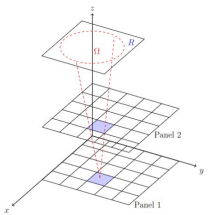

Estimación robusta, preservando los sistemáticos:
Monte Carlo frameworks.

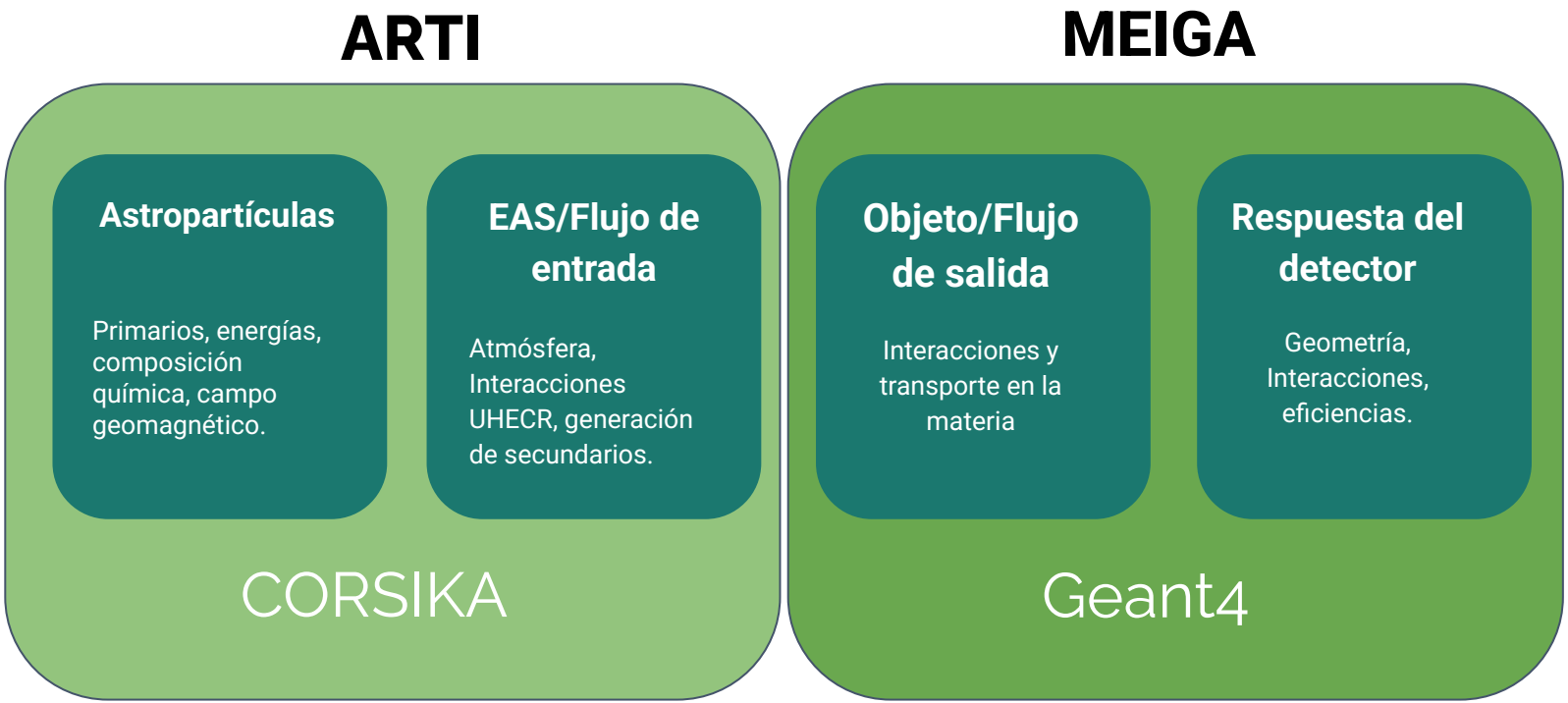

SPOILER: Puede hacerse un atajo!

Cálculo del flujo: Una fuente poco controlada pero muy estudiada.

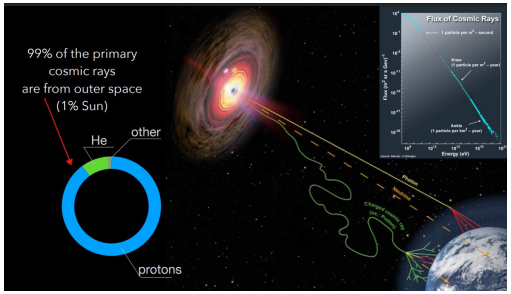

Astropartículas

Primarios, energías, composición química, campo geomagnético.

EAS/Flujo de entrada

Atmósfera, Interacciones UHECR, generación de secundarios.

CORSIKA

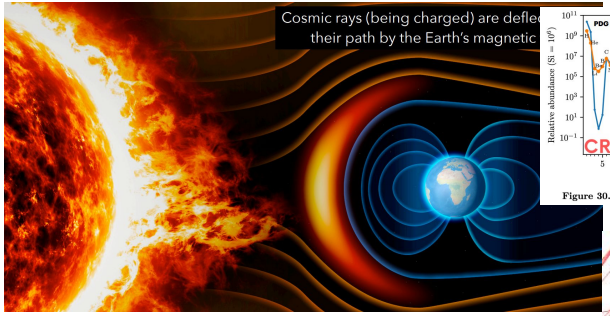

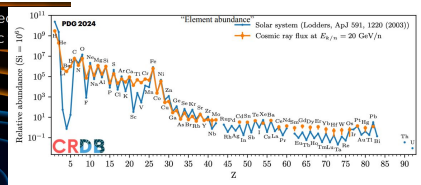

Figure 30.2: CR abundances compared with solar system ones [58]. Modified from [35].

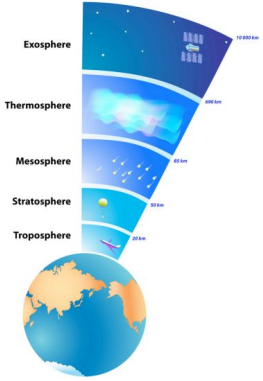

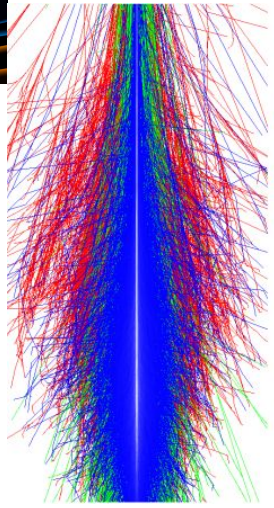

Radiación Cósmica: Partamos de nuestras observaciones.

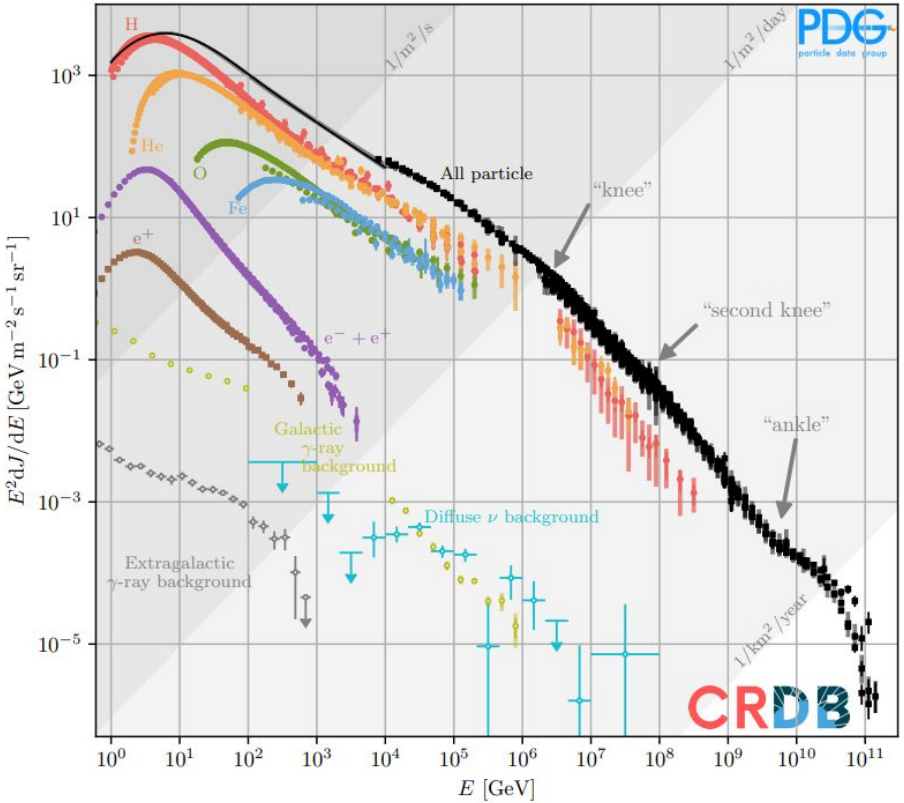

Spectrum (CRs). [Navas et al.(2024)] PDG

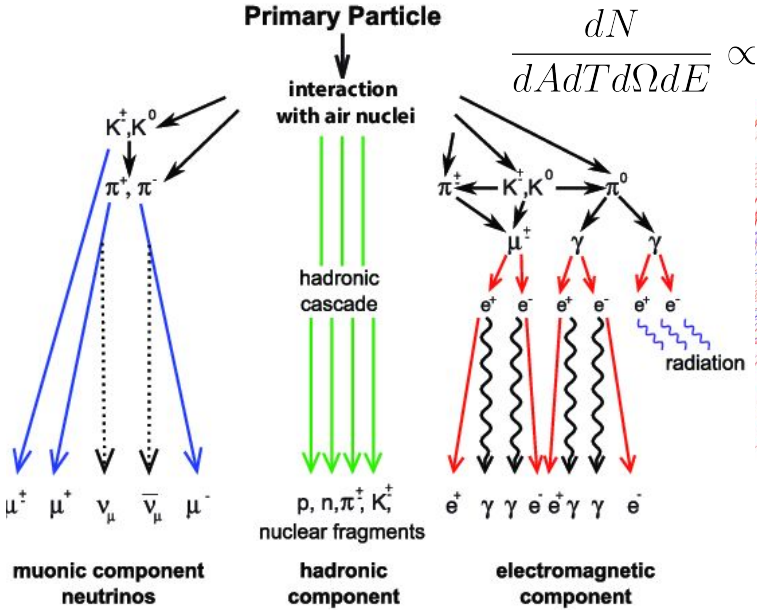

$$\frac{dN}{dAdTd\Omega dE} \propto E^{\eta}$$

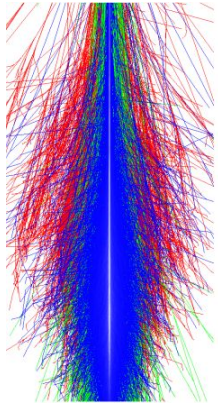

Partícula	Canales de desintegración parcial	BR [%]	Vida media [s]
$\pi^{\pm}$	$\mu^{\pm} + (\nu_\mu)$	99.99	$2.603 \cdot 10^{-8}$
$K^{\pm}$	$\mu^{\pm} + (\nu_\mu)$	63.43	$1.238 \cdot 10^{-8}$
	$\pi^0 + \mu^{\pm} + (\nu_\mu)$	3.27	
$\tau^{\pm}$	$\mu^{\pm} + (\nu_\mu) + (\bar{\nu}_\tau)$	17.36	$2.906 \cdot 10^{-13}$
$D^{\pm}$	$K^0 + \mu^{\pm} + (\nu_\mu)$	7.0	$1.040 \cdot 10^{-12}$
D^0	$\mu^{\pm}$ + Hadrones	6.5	$4.103 \cdot 10^{-13}$
	$K^- + \mu^+ + \nu_\mu$	3.19	

Modelos para EAS: Revisemos 2 aproximaciones al desarrollo de las EAS.

- **Heitler model (1944)**
- **electromagnetic showers in the atmosphere**

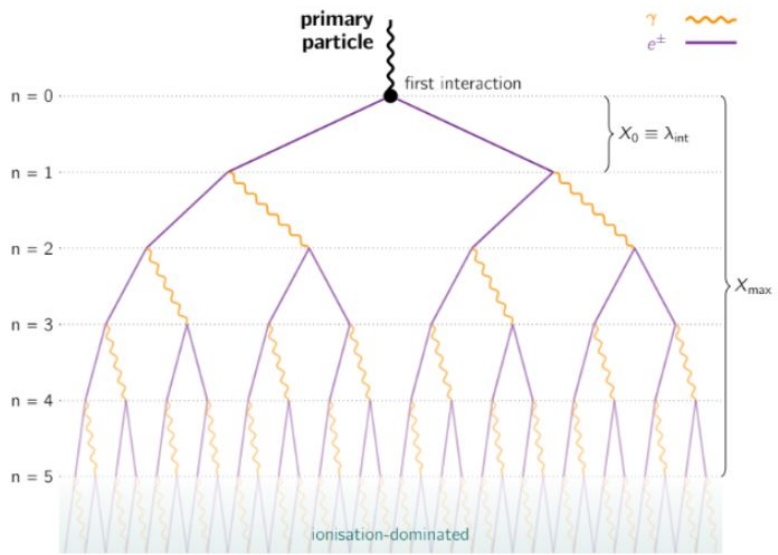

- *bremsstrahlung:*

$$e^{\pm} + {}^{A}_{Z}X \rightarrow e^{\pm} + {}^{A}_{Z}X + \gamma$$

- *Bethe-Heitler pair production:*

$$\gamma + {}^{A}_{Z}X \rightarrow e^{+} + e^{-} + {}^{A}_{Z}X$$

- *ionisation losses*

maximum number of particles:

$$N_{\max} = \frac{E_0}{E_c}$$

depth of the shower maximum:

$$X_{\max} = X_0 \log_2\left(\frac{E_0}{E_c}\right)$$

the Heitler-Matthews model for air showers

- **Heitler-Matthews model** (2005)
- **hadronic showers** in the atmosphere
- interplay of:
  - hadronic interactions
  - pion decay
  - all processes of electromagnetic showers
- 2/3 of the shower is hadronic, 1/3 electromagnetic
- depth of the shower maximum:

$$X_{\max} = \lambda_{\text{int}} + X_0 \log_2 \left(\frac{1}{3} \frac{E_0}{E_{\pi,c}} \right)$$

- **number of muons:**

$$N_\mu \propto \left(\frac{E_0}{E_c} \right)^{0.9}$$

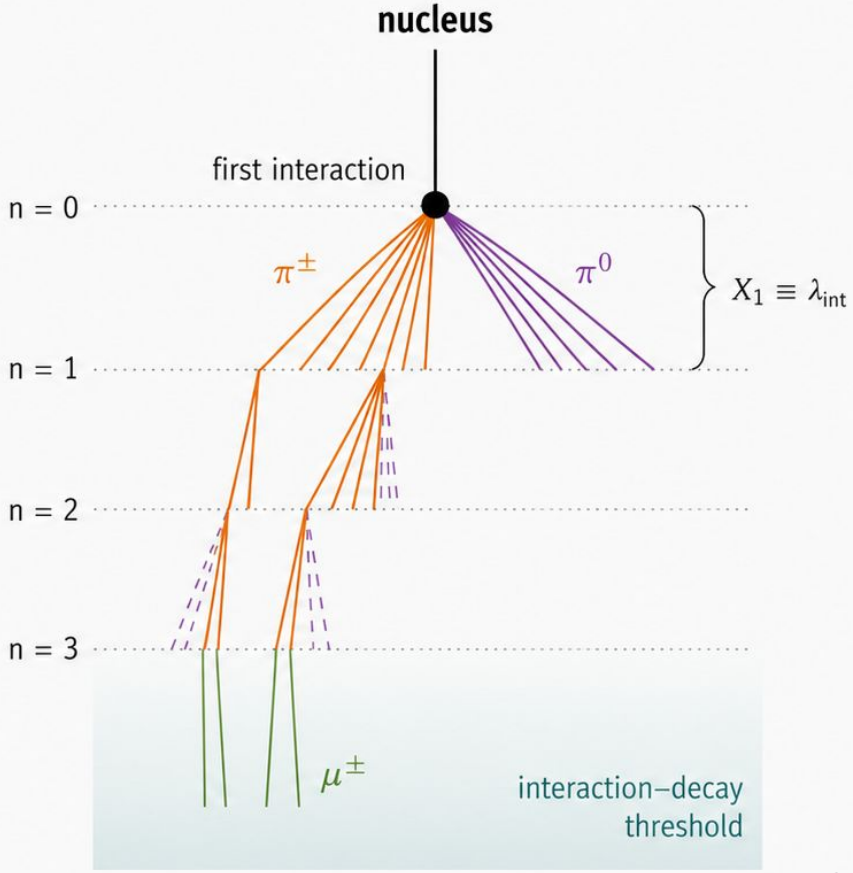

Medidas: Los observables de interés son espectros **energéticos** y **angulares**

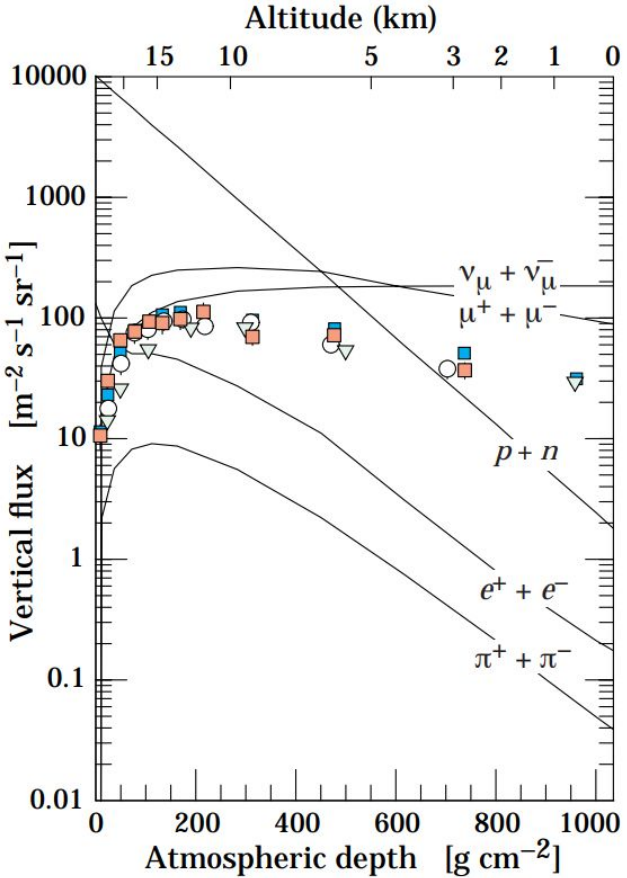

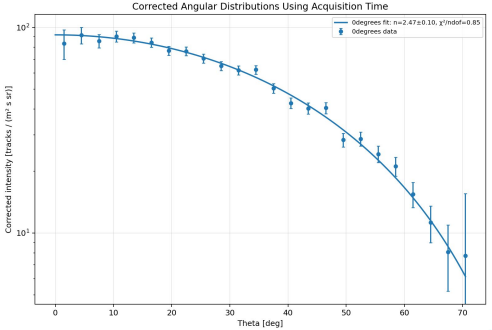

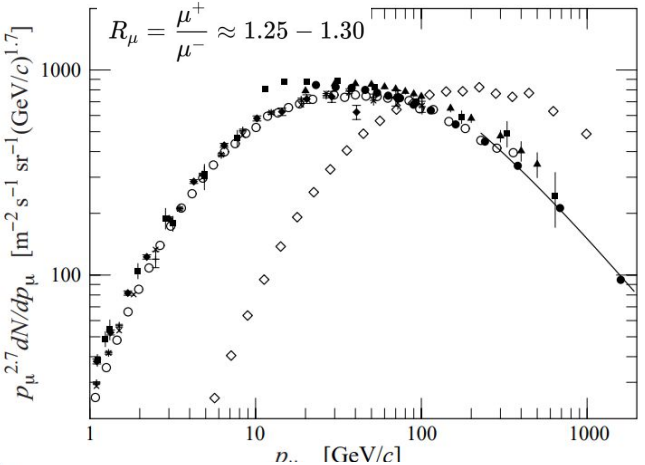

MINOS Near Detector midió:

$$R_\mu = 1.266 \pm 0.001(\text{stat.})^{+0.015}_{-0.014}(\text{syst.})$$

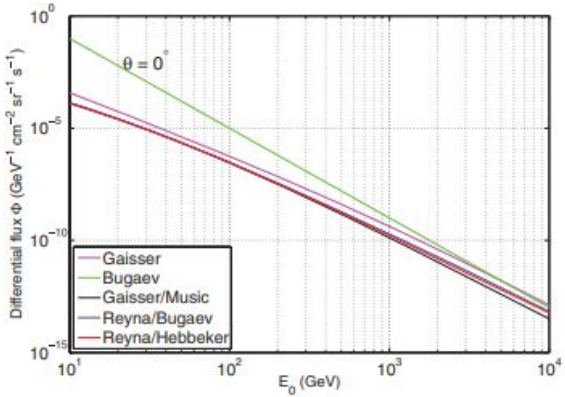

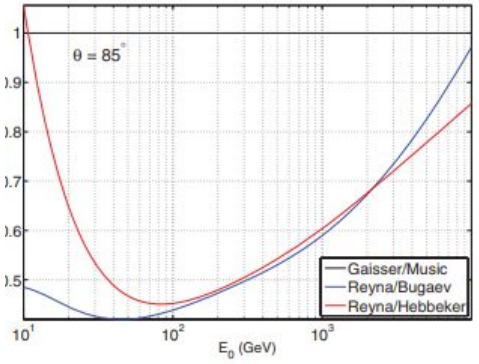

CORSIKA:Cosmic **R**ay **Si**mulation for **KA**SCADE

KASCADE: an experiment to measure the composition of cosmic rays in Karlsruhe (Germany) 1997-2009

- EM model: EGS4 Low energy
- hadronic models: FLUKA UrQMD GHEISHA
- High energy hadronic models: QGSJET EPOS-LHC DPMJET SIBYLL

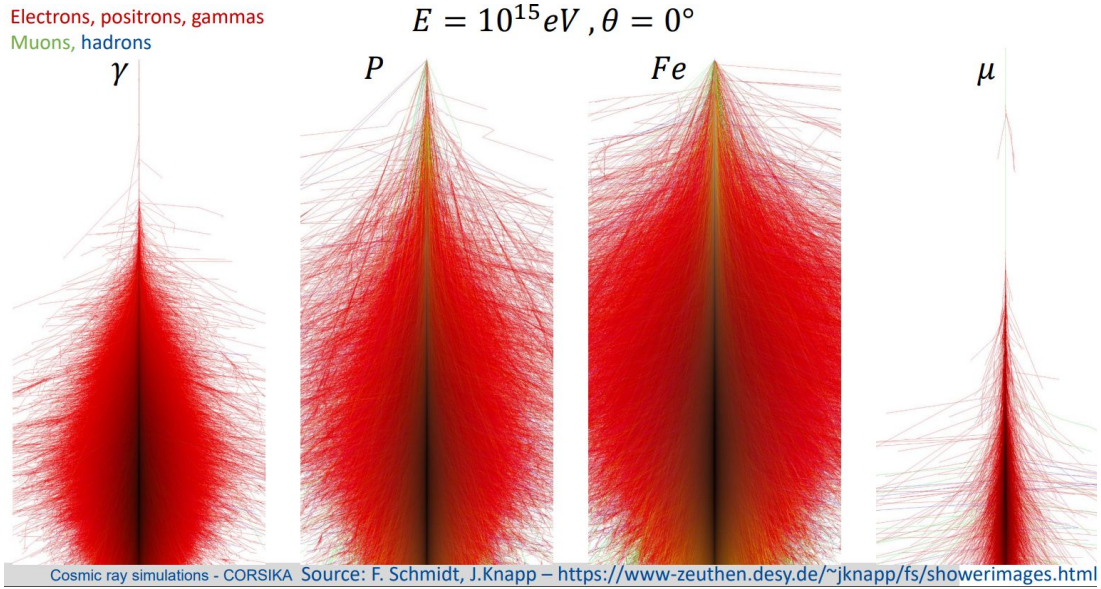

Tuned at collider energies (TeV) and extrapolated to 10^{20} eV

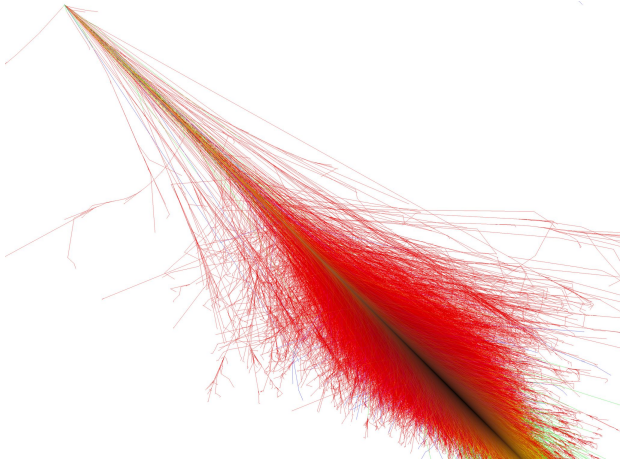

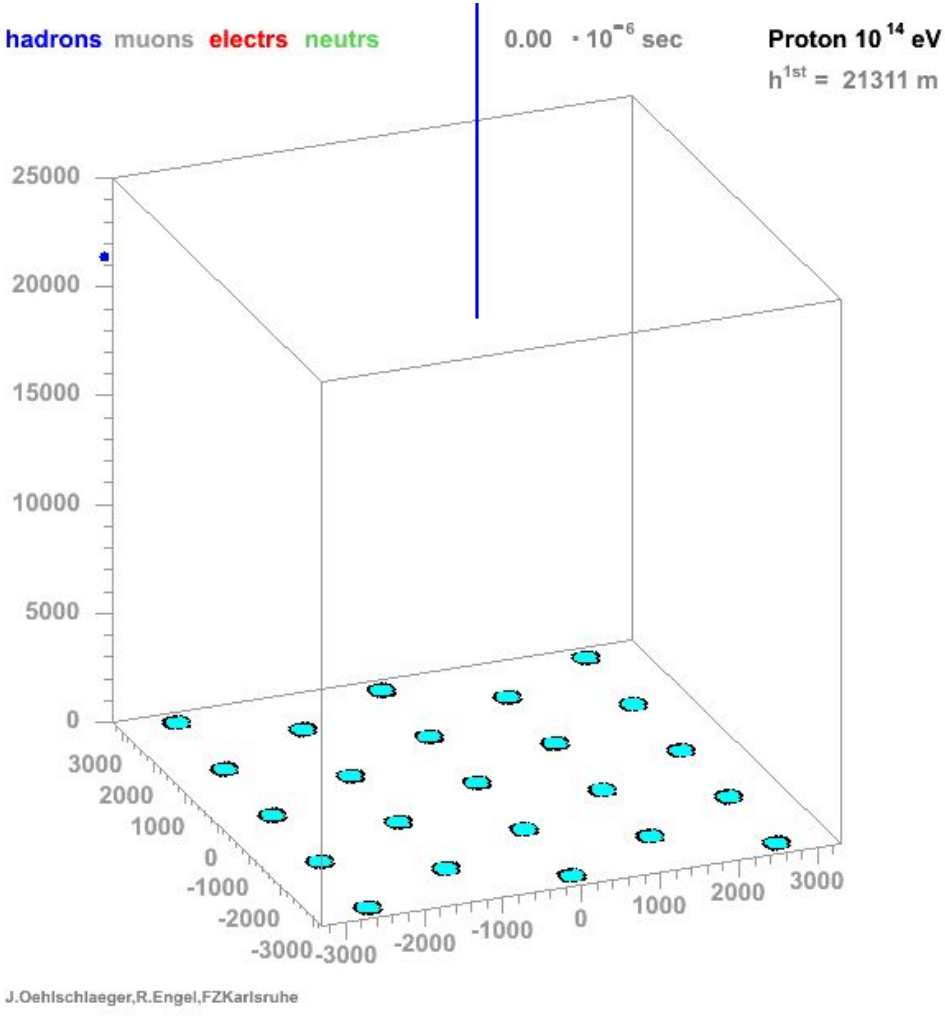
hadrons muons electrs neutrs
0.00 · 10^-6 sec
Proton 10^14 eV
h^1st = 21311 m
25000
20000
15000
10000
5000
0
3000
2000
1000
0
-1000
-2000
-3000
-3000 -2000 -1000 0 1000 2000 3000
J.Oehlschlaeger,R.Engel,FZKarlsruhe

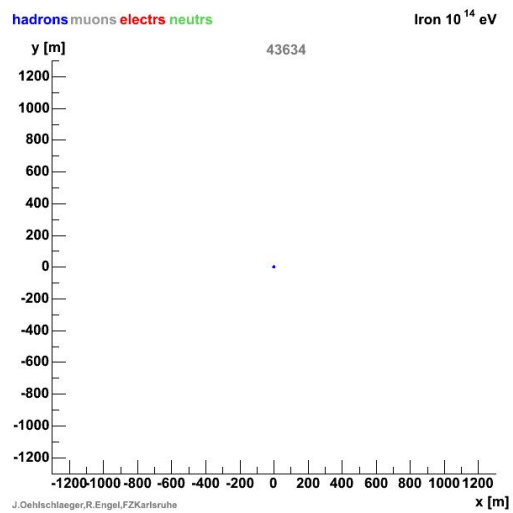
hadrons muons electrs neutrs
Iron 10^14 eV
y [m]
43634
1200
1000
800
600
400
200
0
-200
-400
-600
-800
-1000
-1200
-1200 -1000 -800 -600 -400 -200 0 200 400 600 800 1000 1200
x [m]
J.Oehlschlaeger,R.Engel,FZKarlsruhe

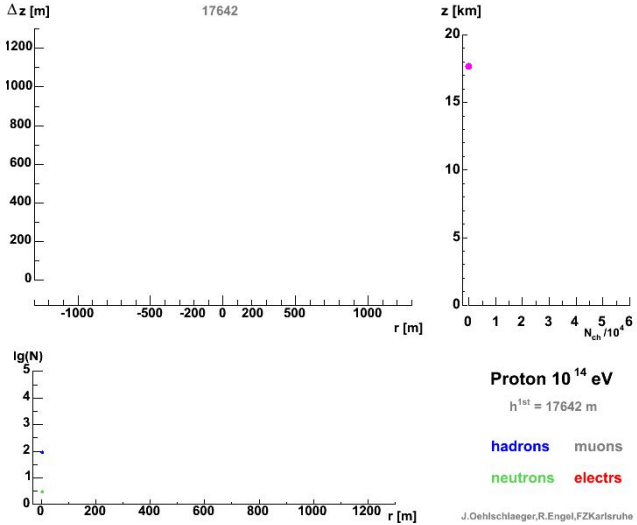
Δz [m]
17642
1200
1000
800
600
400
200
0
-1000 -500 -200 0 200 500 1000
r [m]
z [km]
20
15
10
5
0
0 1 2 3 4 5 6
N_ch /10^4
lg(N)
5
4
3
2
1
0
0 200 400 600 800 1000 1200
r [m]
Proton 10^14 eV
h^1st = 17642 m
hadrons muons
neutrons electrs
J.Oehlschlaeger,R.Engel,FZKarlsruhe

CORSIKA: Software consolidado en la comunidad científica

HAWC
High Altitude Water Cherenkov
Gamma-Ray Observatory

LHAASO
高海拔宇宙线观测站

KIT
Karlsruhe Institute of Technology

KCDC

PIERRE AUGER OBSERVATORY

H.E.S.S.

Sin embargo…

… para la muografía nos interesa el flujo de secundarios generados por los primarios

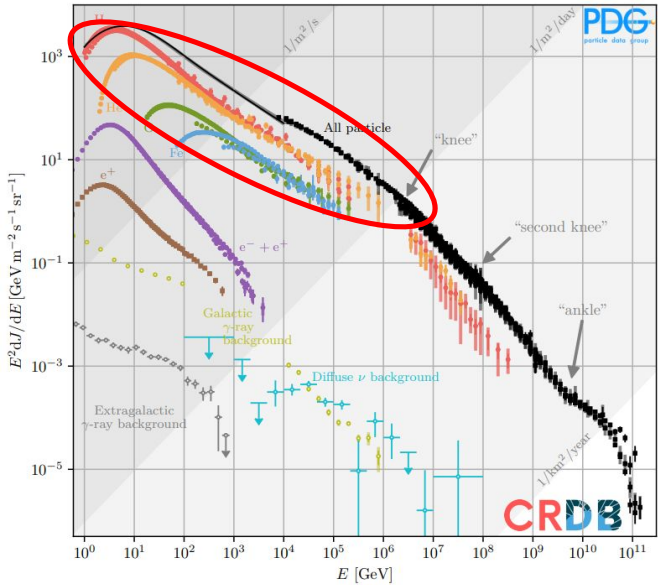

Spectrum (CRs). [Navas et al.(2024)] PDG

Flux Estimation: ARTI framework Monte Carlo/CORSIKA based.

Provides the reference site-dependent muon flux. The generative model learns to reproduce it quickly.

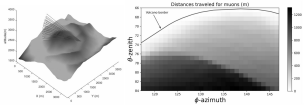

Volcano	Criterion 1:	Criterion 2:	Criterion 3:
Ámbrai	N	Y	N
Cerro Negro*	Y	Y	N
Chiles*	Y	Y	N
Cumbal	N	Y	N
Doña Juana	N	Y	N
Galeras	Y	N	Y
Machín	**Y**	**Y**	**Y**
Nevado del Huila	N	Y	N
Nevado del Ruiz	N	Y	Y
Nevado Santa Isabel	N	Y	Y
Nevado del Tolima	N	N	Y
Puracé	N	Y	Y
Sotará	N	Y	N

Vesga-Ramírez, A., et al (2020). **Muon**

Primary flux integration from observations at 112 km.

$$\Phi(E_p,Z,A,\Omega)=j_0(Z,A)\left(\frac{E_p}{E_0}\right)^{\alpha(E_p,Z,A)}$$

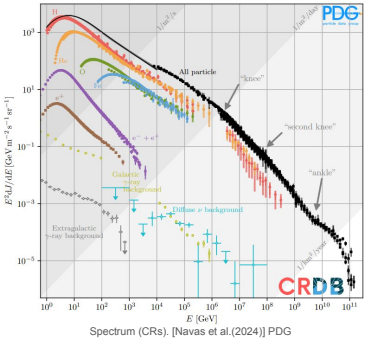

Spectrum (CRs). [Navas et al.(2024)] PDG

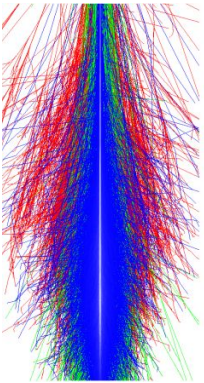

CORSIKA simulation for all the primaries particles with site depend condition

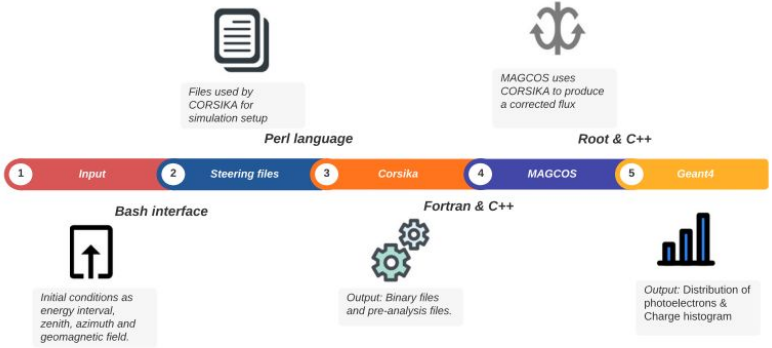

Sarmiento-Cano, & LAGO Collaboration. (2022). **The ARTI framework: cosmic rays atmospheric background simulations**. *The European Physical Journal C*, *82*(11), 1019.

Recording of the secondary particles generated

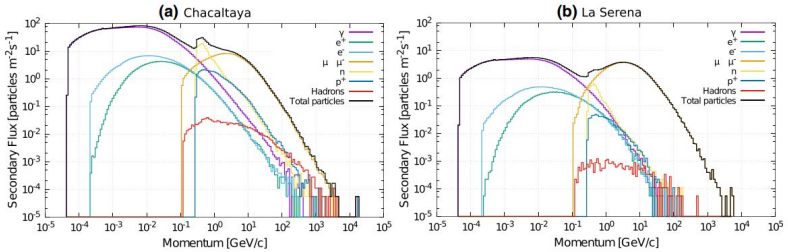

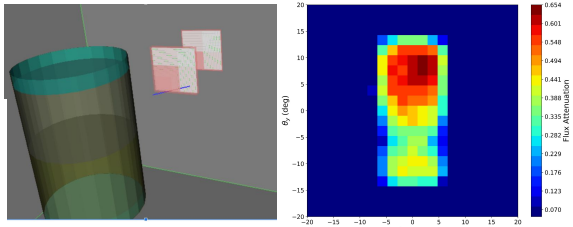

R. A. Martínez-Rivero, et al. (2025); M**uon imaging of hydrotreatment reactors.** *J. Appl. Phys.*

- El flujo de partículas secundarias varía con la **altitud**, el **campo geomagnético local** y el **perfil atmosférico**.
- Por ello, cada ubicación presenta un **espectro de fondo distinto**.
- En consecuencia, el fondo secundario debe evaluarse **individualmente para cada sitio de observación**.

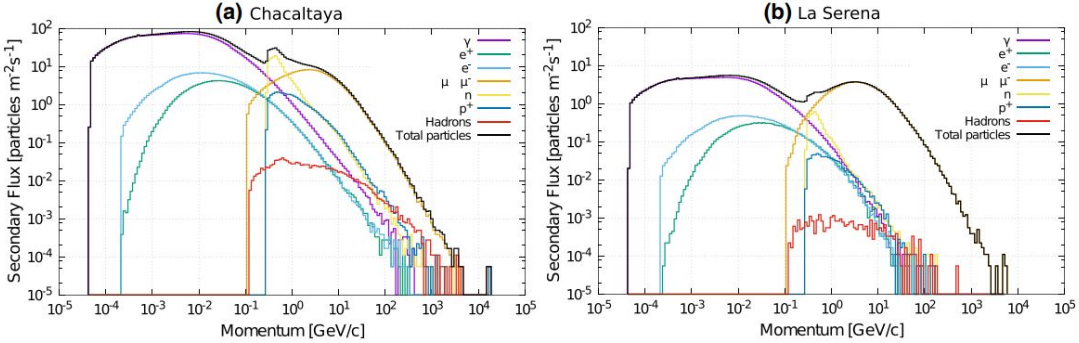

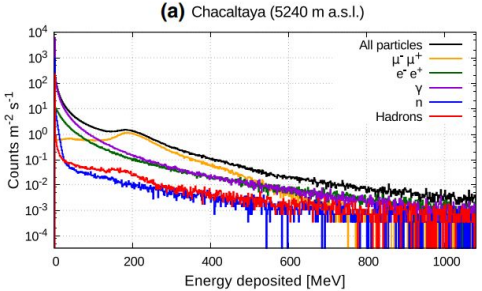

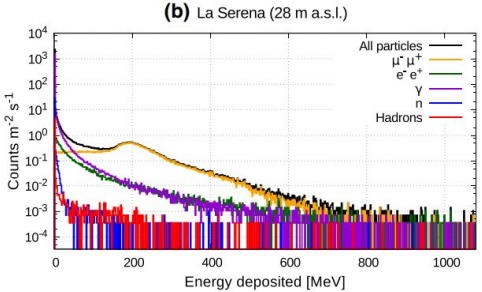

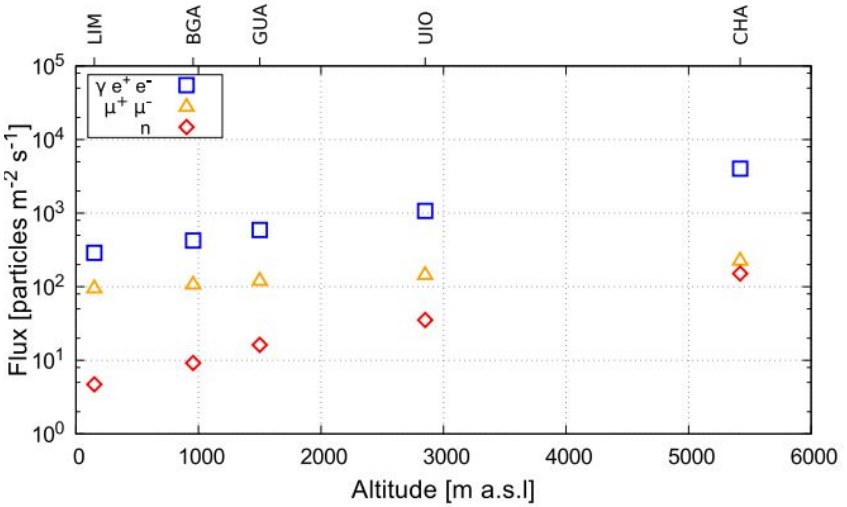

ARTI Simulation framework

Sarmiento-Cano, & LAGO Collaboration. (2022). **The ARTI framework: cosmic rays atmospheric background simulations**. *The European Physical Journal C*, *82*(11), 1019.

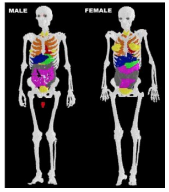

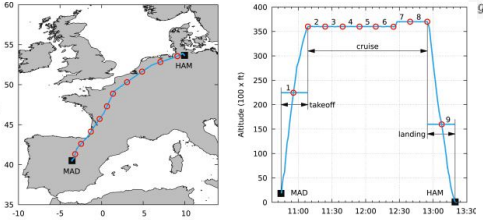

Asorey, H., Suárez-Durán, M., & Mayo-García, R. (2023). **ACORDE: A new application for estimating the dose absorbed by passengers and crews in commercial flights**. *Applied Radiation and Isotopes*, *196*, 110752.

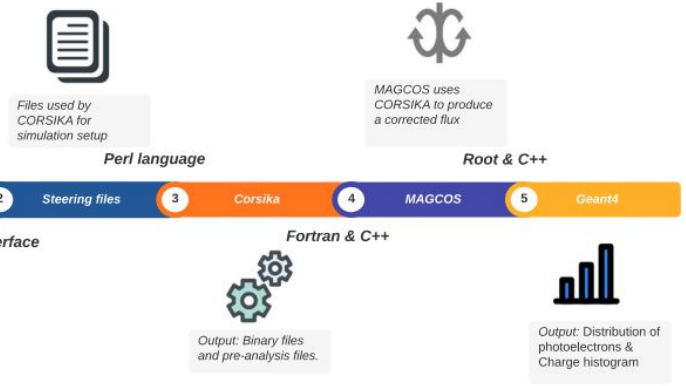

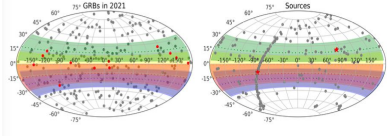

Sidelnik, I.,& LAGO Collaboration. (2023). **The capability of water Cherenkov detectors arrays of the LAGO project to detect Gamma-Ray Burst and high energy astrophysics sources.** *Nuclear Instruments and Methods in Physics Research 1056*, 168576.

Country	Site	Altitude [m asl]	Latitude [deg]	Longitude [deg]
Sierra Negra	SNG	4,550	18.2 N	97.9 W
Chimborazo	CHI	5,000	1.5 S	78.8 W
Imata	IMA	4,600	15.9 S	71.1 W
Atacama	ATA	5,100	23.0 S	67.8 W
S. A. de los Cobres	SAC	4,500	24.2 S	66.3 W

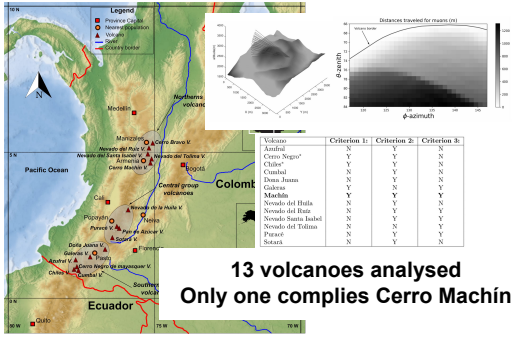

13 volcanoes analysed
Only one complies Cerro Machín

Vesga-Ramírez, A., et al (2020). **Muon Tomography sites for Colombian volcanoes.** *ANNALS OF GEOPHYSICS*, *63*(6).

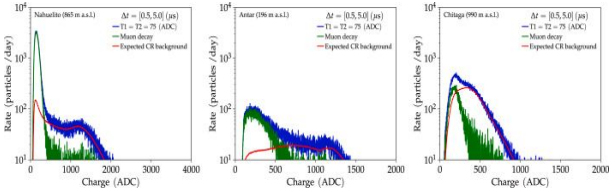

Otiniano, L.,& LAGO Collaboration. (2023). **Measurement of the muon lifetime and the Michel spectrum in the LAGO water Cherenkov detectors as a tool to enhance the signal-to-noise ratio.** *Nuclear Instruments and Methods in Physics Research 1056*, 168567.

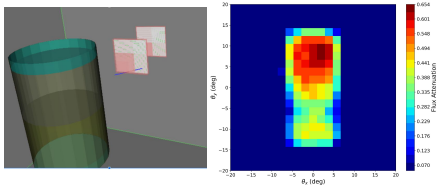

R. A. Martínez-Rivero, C. Sarmiento-Cano, D. Castillo-Morales, J. Perea-Pérez, V. G. Baldovino-Medrano, J. D. Sanabria-Gómez, L. A. Núñez; Muon imaging of hydrotreatment reactors. *J. Appl. Phys.* 28 December 2025; 138 (24): 244901. https://doi.org/10.1063/5.0281667

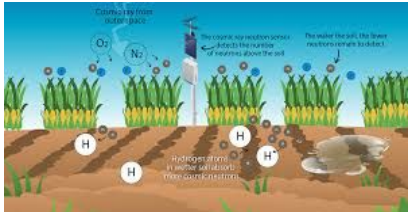

J. Betancourt, et al. (2025) Enhanced water Cherenkov detector for soil moisture detection. https://doi.org/10.48550/arXiv.2509.08562

MEIGA

Objeto/Flujo de salida

Interacciones y transporte en la materia

Respuesta del detector

Geometría, Interacciones, eficiencias.

Geant4

What is MEIGA

What is it?

MEIGA is a framework based on C++ classes. It combines three elements:

- Cosmic-ray flux calculation
- Particle propagation
- Detector response simulation

How does it work?

- Uses **JSON configuration files** (input/output paths, detector setup, physics lists, verbosity).
- Runs **Geant4 simulations**, injecting particles at ground level.
- Tracks particles inside the detector geometry defined by XML files.
- Collects detector response (energy deposits, SiPM signals, time traces).

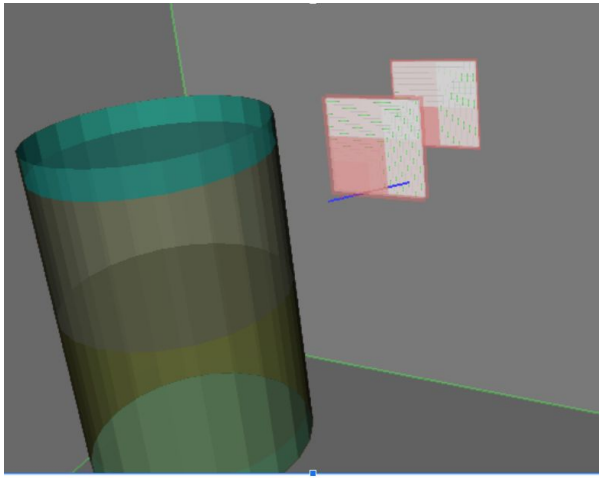

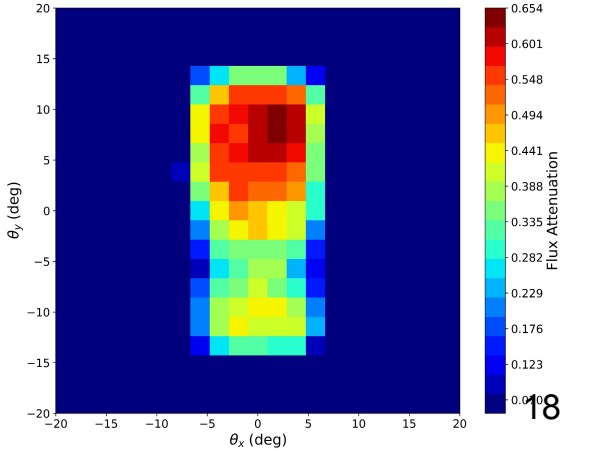

The core of MEIGA is GEANT4

- Toolkit to simulate **particle interactions with matter**.
- Uses databases, cross-sections, and physics models.
- Widely used in **HEP, medical physics, and space science**.

Key Features

- **Physics List**
  - Define particles
  - Define processes
- **Detector Construction**
  - Define materials
  - Build geometry
  - Set sensitive regions
- **User Action Classes**
  - Generate primary particles
  - Extract data (energy, tracks, steps)

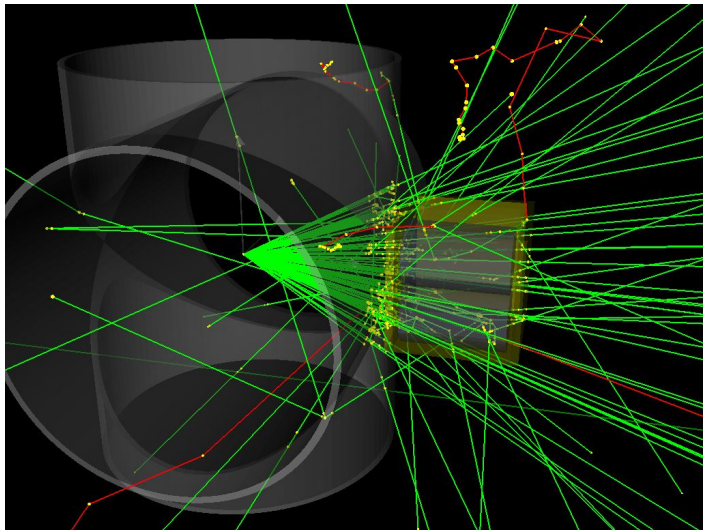

Meiga Application (users)

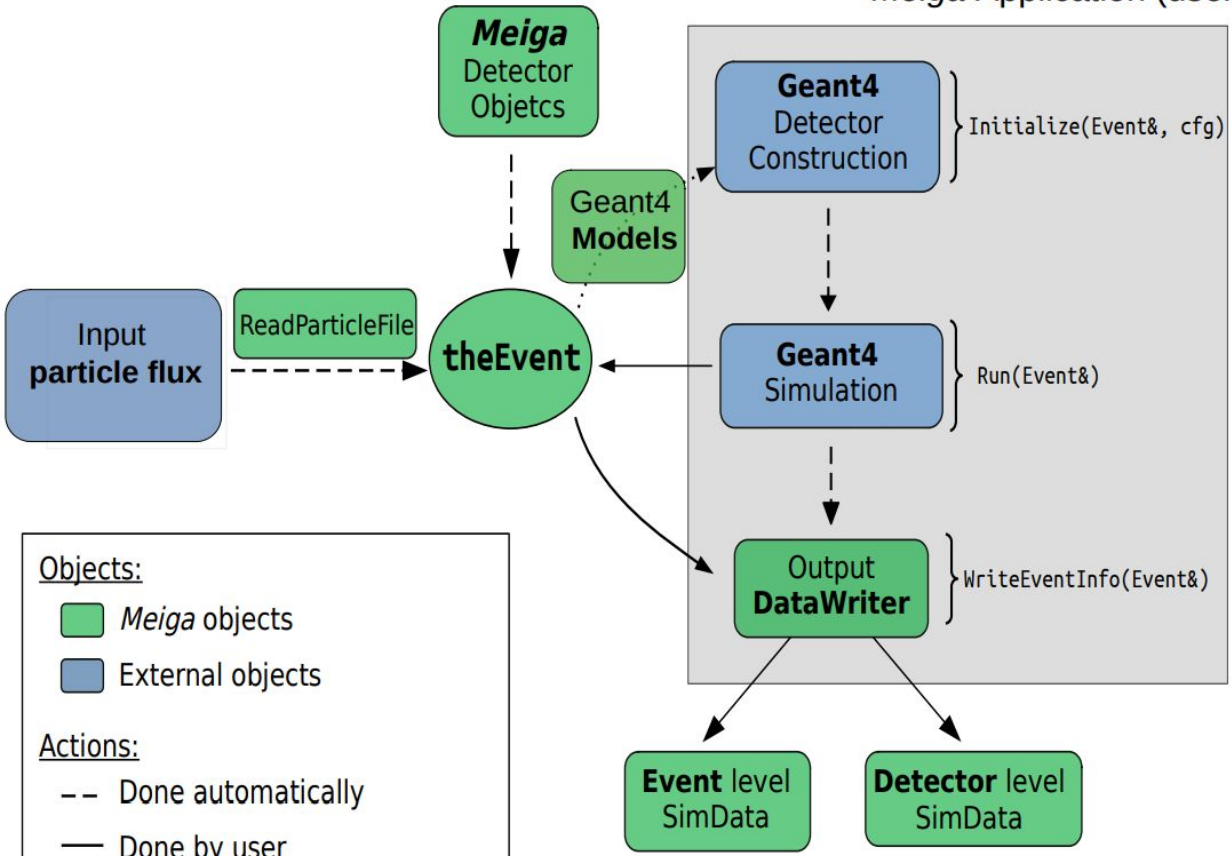

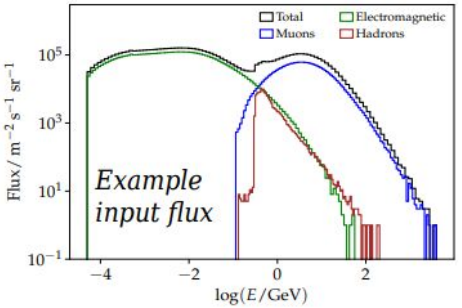

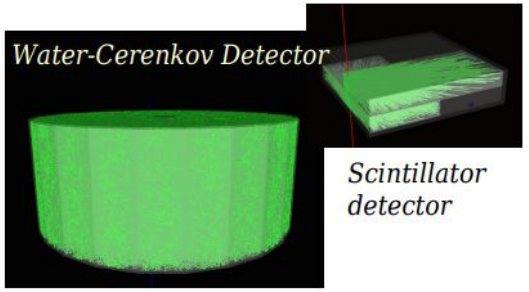

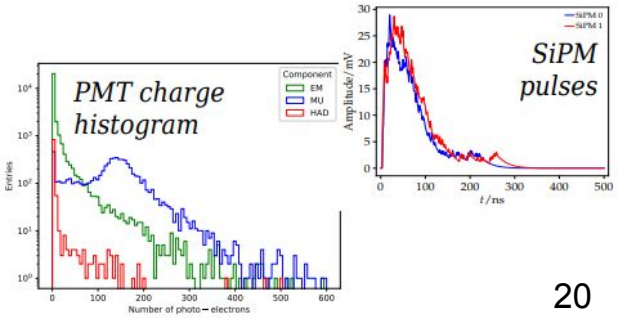

Modelado del detector

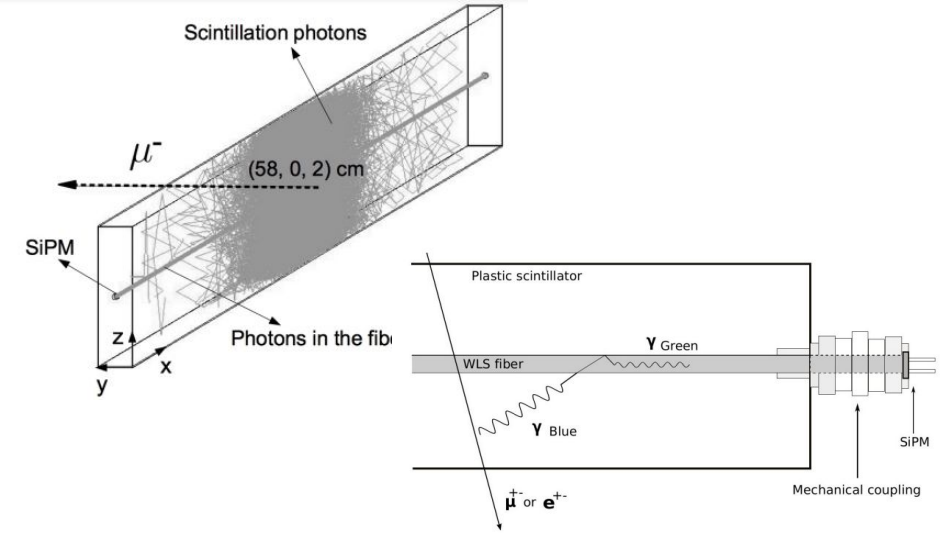

- **Diseño geométrico**: Barras de centelleo organizadas en un arreglo **NxN** distribuidas en dos paneles perpendiculares.
- **Dimensiones de las barras**: Ancho, longitud y grosor ajustados según la simulación.
- **Carcasa externa**: Protege y afecta el comportamiento óptico de la luz emitida.

Propiedades Ópticas del Centelleador

- **Energía de los fotones**: 2.00 eV a 4.20 eV.
- **Índice de refracción**: Constante de 1.5.
- **Longitud de absorción**: 4 cm a 24 cm, dependiendo de la energía.
- **Componentes rápidas y lentas**: Simulación de respuesta temporal.

Fibras Ópticas y Detección

- **Transporte de fotones**: Fibras ópticas de PMMA con índice de refracción de 1.60.
- **Detección óptica**: Fotomultiplicadores con modelado preciso de su eficiencia cuántica.

Reflexión y Dispersión

- **Rugosidad superficial**: Control de la dispersión de fotones.
- **Reflexión especular**: 20% de la luz reflejada en un lóbulo especular, sin reflexión especular exacta.

Sensor Óptico SiPM

Blindaje de Pb con densidad 11.3 g/cm³

Simular para diseñar

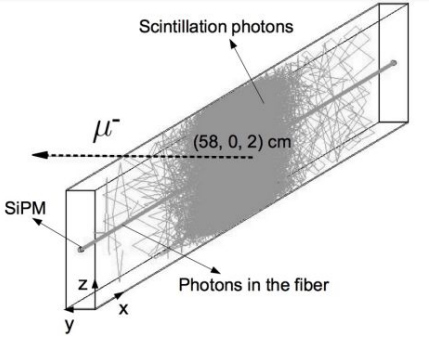

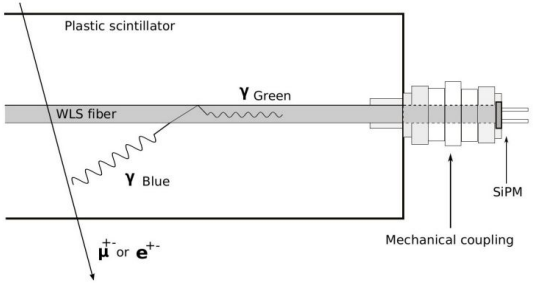

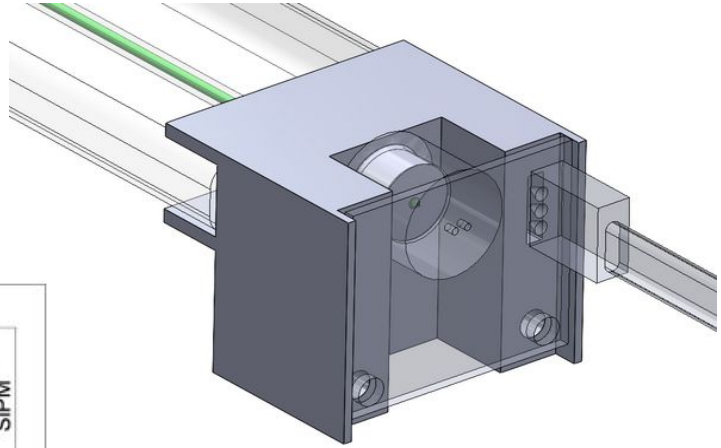

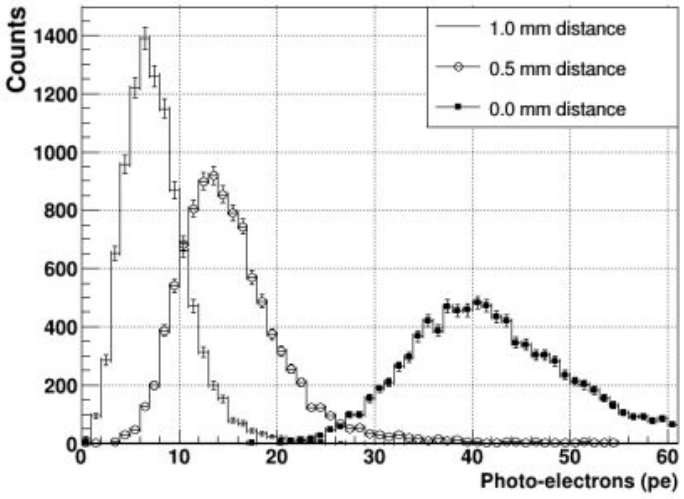

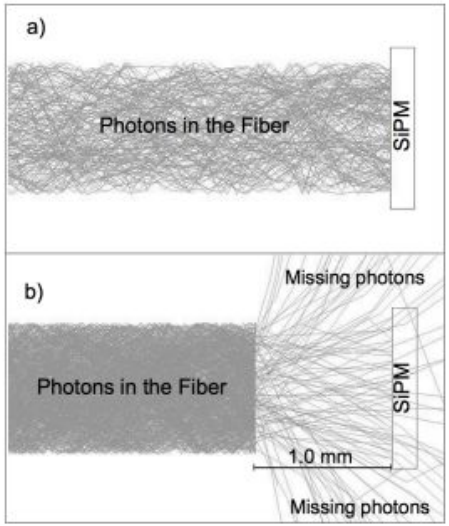

Acople MuTe 2.0

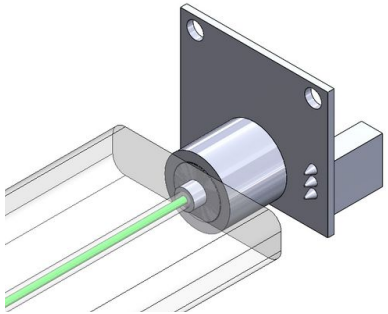

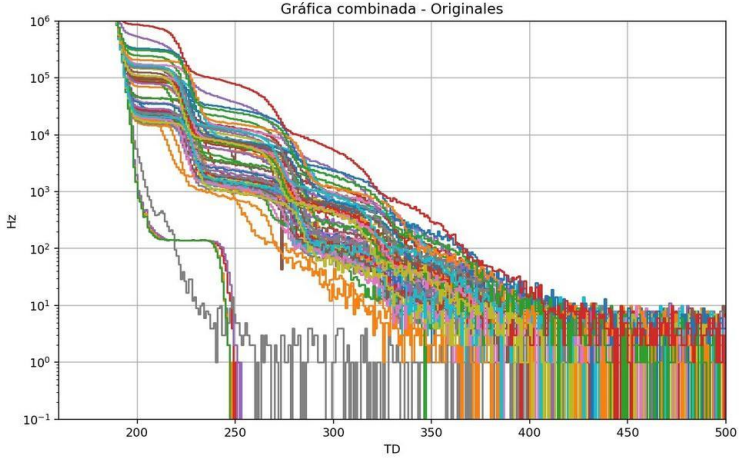

Acople

Alternativa **C**

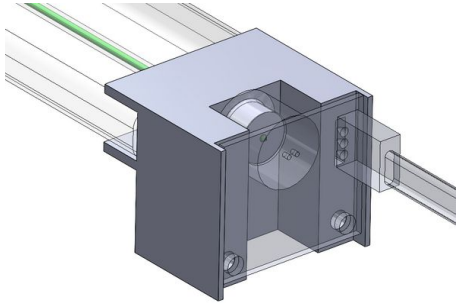

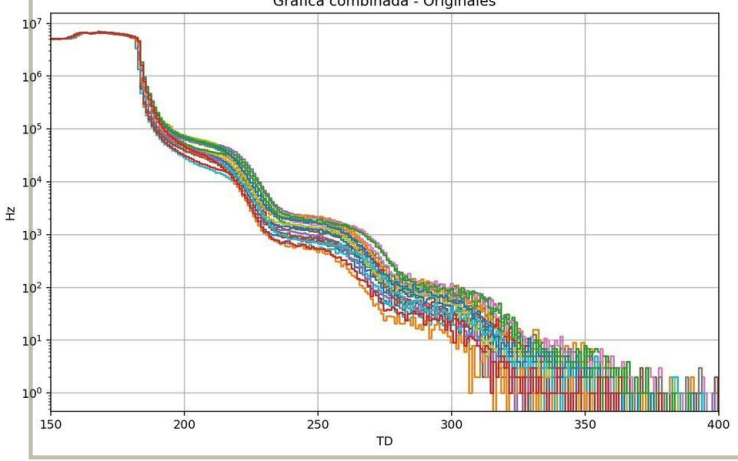

Problema directo: Cadena de procesos = Cadena de simulaciones

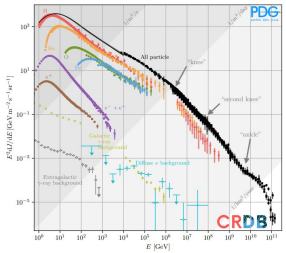

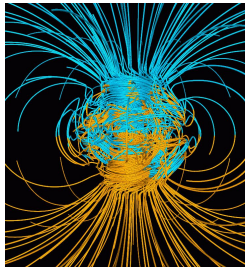

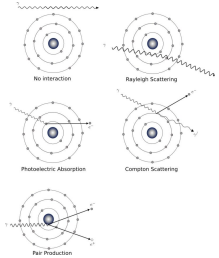

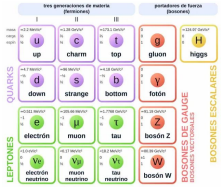

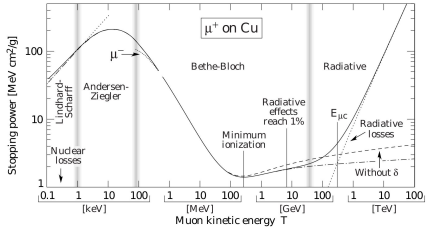

Astropartículas

Primarios, energías, composición química, campo geomagnético.

EAS/Flujo de entrada

Atmósfera, Interacciones UHECR, generación de secundarios.

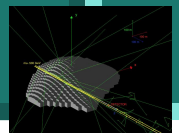

Objeto/Flujo de salida

Interacciones y transporte en la materia

Respuesta del detector

Geometría, Interacciones, eficiencias.

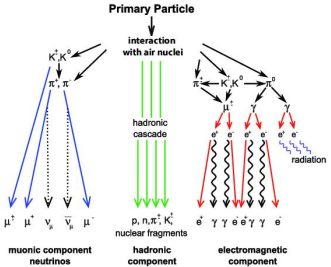

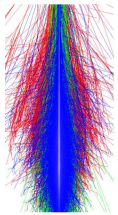

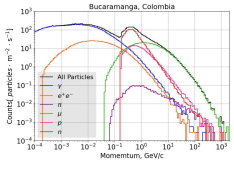

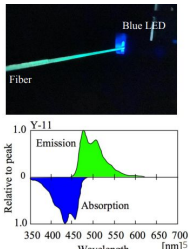

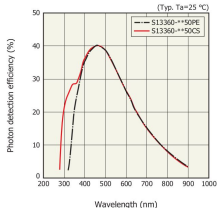

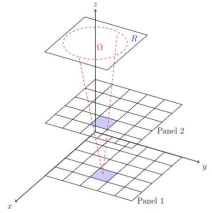

Aplicación particular: Exploring muon imaging in reactors

Height: 20-40 m (some reach over 50 m)
Diameter: 3-6 m

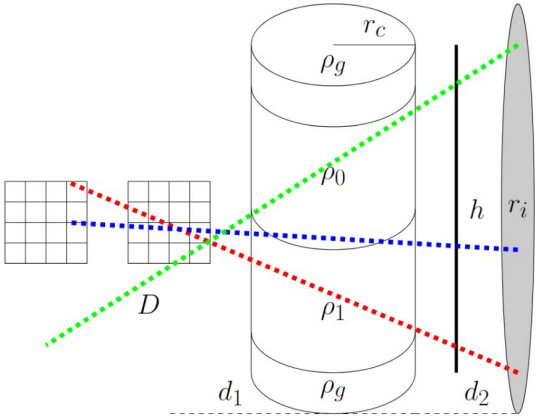

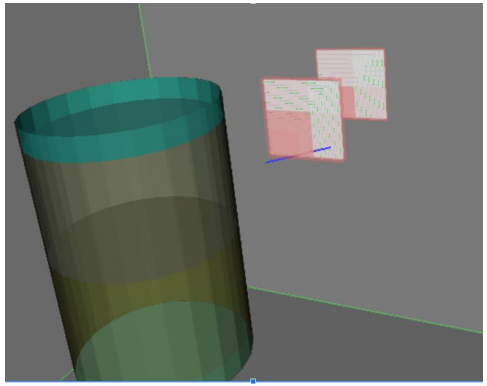

Framework validation with measurement

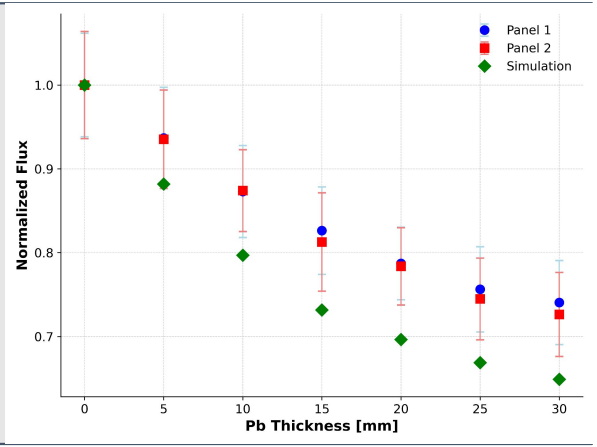

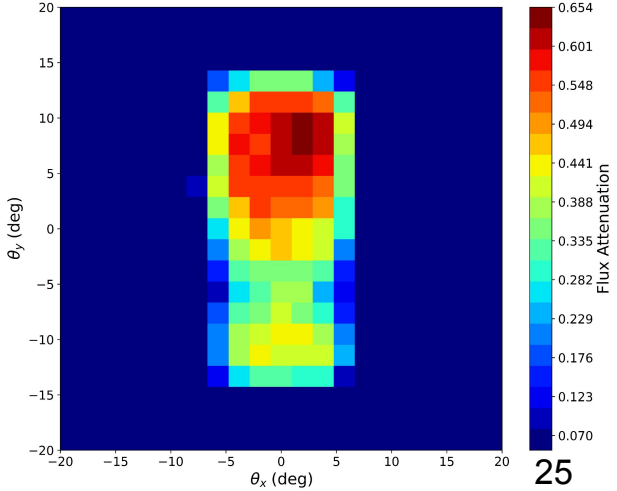

R. A. Martínez-Rivero, C. Sarmiento-Cano, D. Castillo-Morales, J. Perea-Pérez, V. G. Baldovino-Medrano, J. D. Sanabria-Gómez, L. A. Núñez; Muon imaging of hydrotreatment reactors. *J. Appl. Phys.* 28 December 2025; 138 (24): 244901. https://doi.org/10.1063/5.0281667

Validación reconstrucción

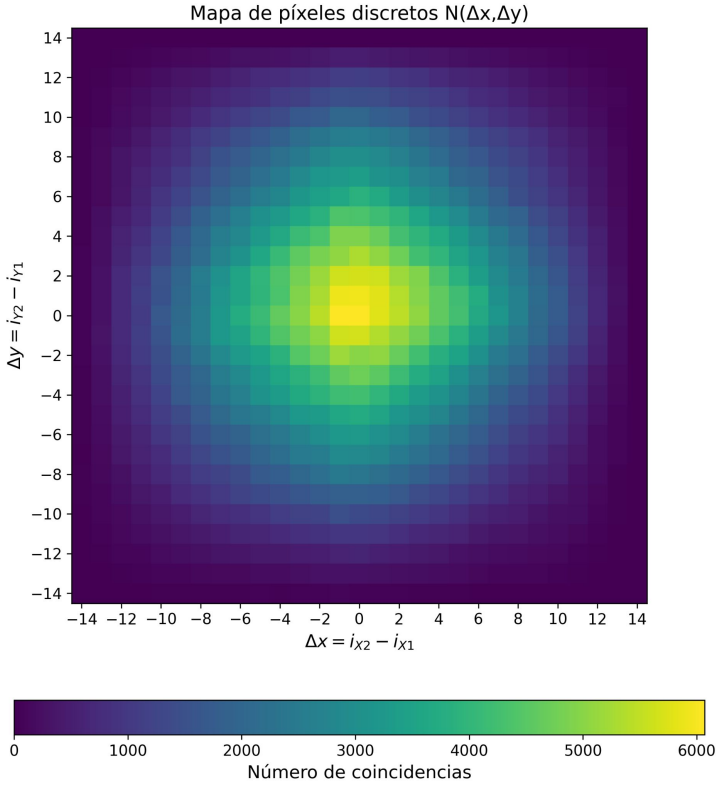

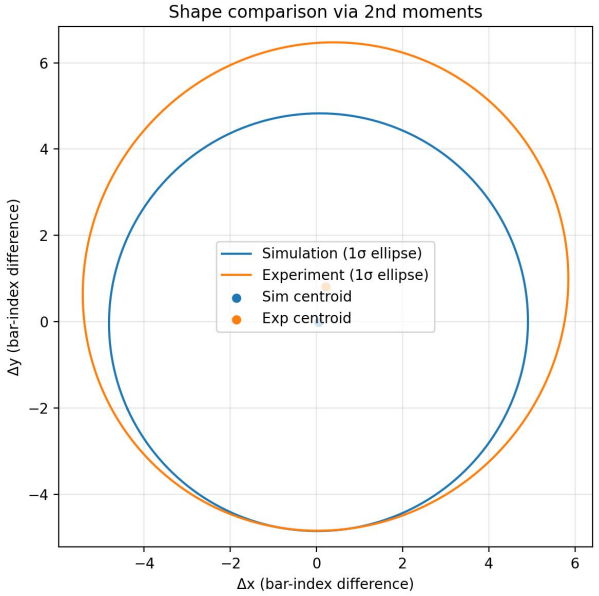

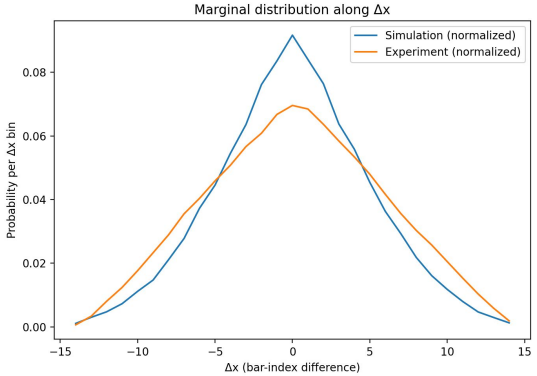

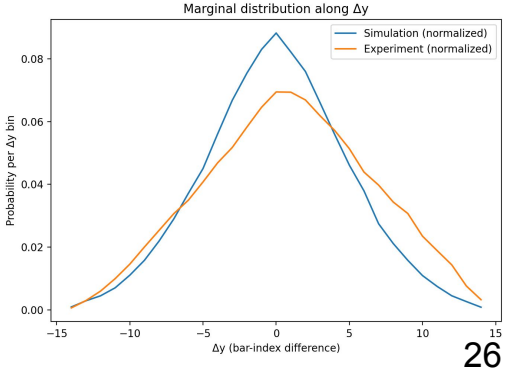

Canales activados por evento

Pico en 2 barras confirma detección de trayectorias limpias.

- Diferencias: más eventos de 1 barra en datos experimentales.
- Causa principal: dark count en SiPM + partículas poco energéticas.

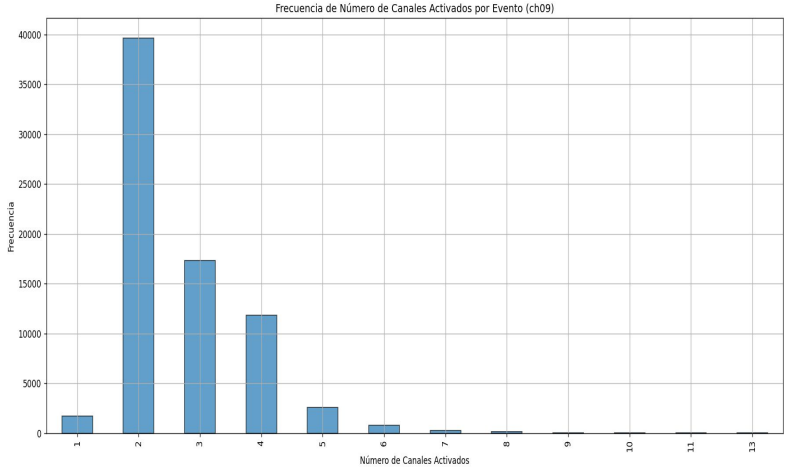

Simulación

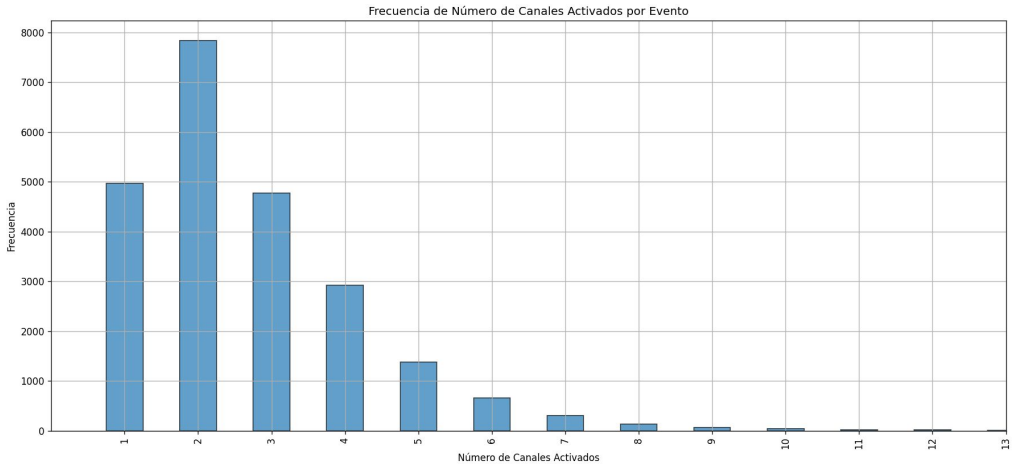

Medición

The Forward Problem in Muography simulation

air-shower source (CORSIKA)

Particle interactions and transport

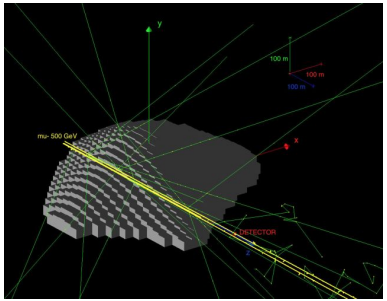

Detector response

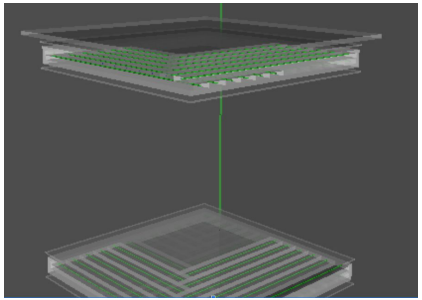

Muogram

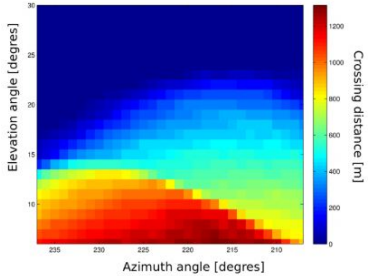

Monte Carlo is detailed but expensive

The Forward Problem in Muography simulation

air-shower source (CORSIKA)

Particle interactions and transport

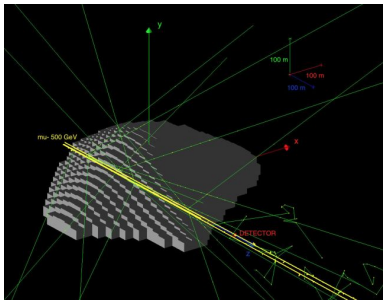

Detector response

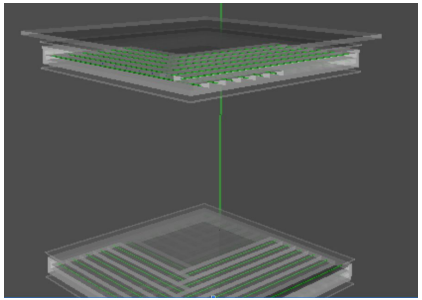

Muogram

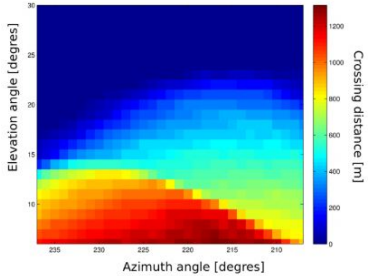

Monte Carlo is detailed but expensive

How can we keep the key physics without running a full Monte Carlo every time?

The Forward Problem in Muography simulation

air-shower source (CORSIKA)

Particle interactions and transport

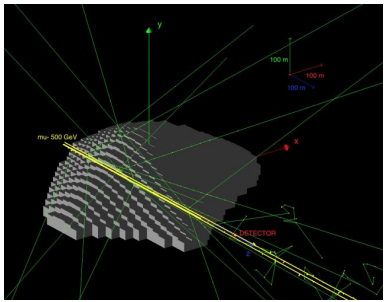

Detector response

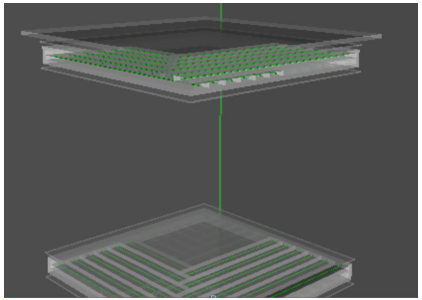

Muogram

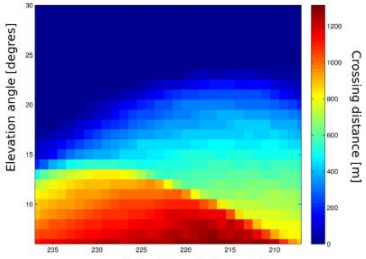

Monte Carlo is detailed in physics but it is expensive

How can we keep the key physics without running a full Monte Carlo every time?

Deep learning muon flux

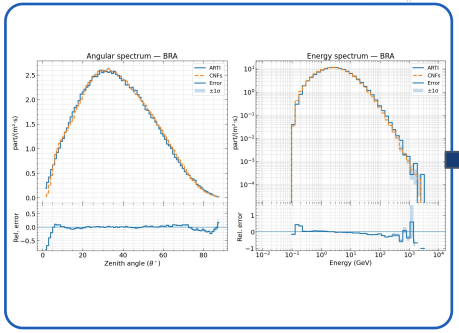

Backpropagation

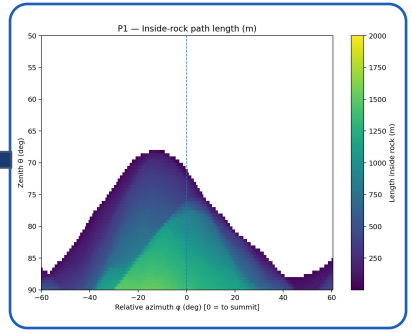

Angular Scattering

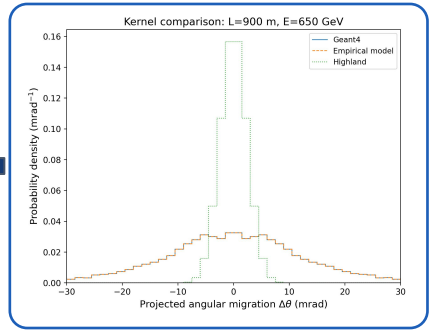

muogram

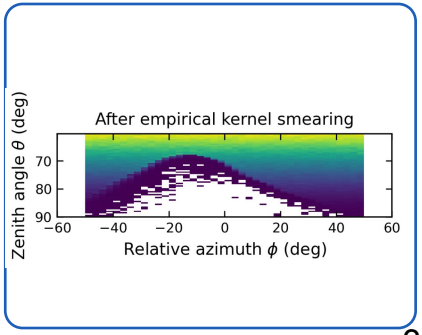

From Monte Carlo simulation to fast AI flux generation

We use CORSIKA outputs as training data, so the AI model can generate muon fluxes faster.

- Monte Carlo simulation gives the reference muon-flux data.
- The training sites cover different altitude and geomagnetic conditions.
- The AI model learns site-dependent angular and energy spectra.
- The generated flux becomes the input of the forward model.

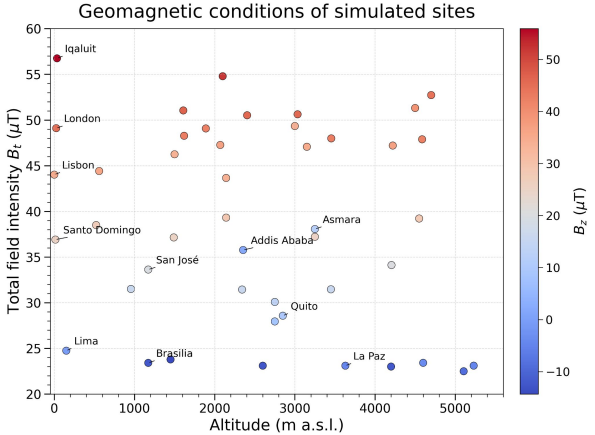

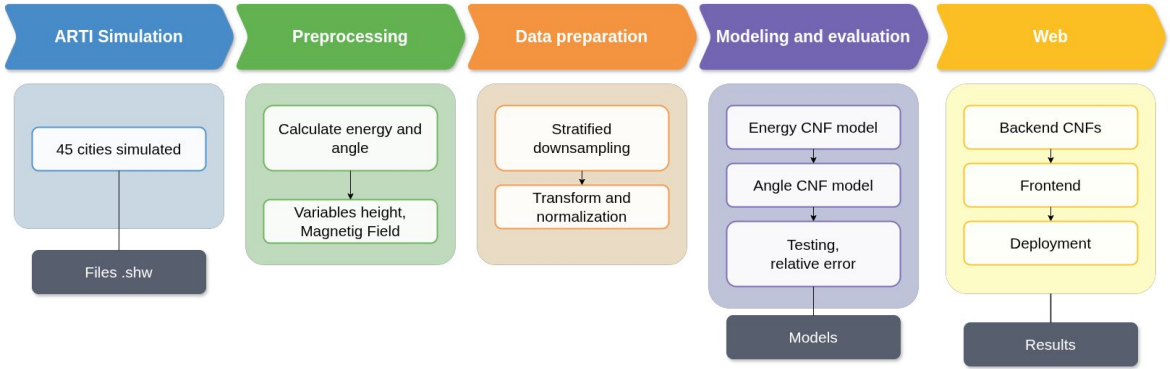

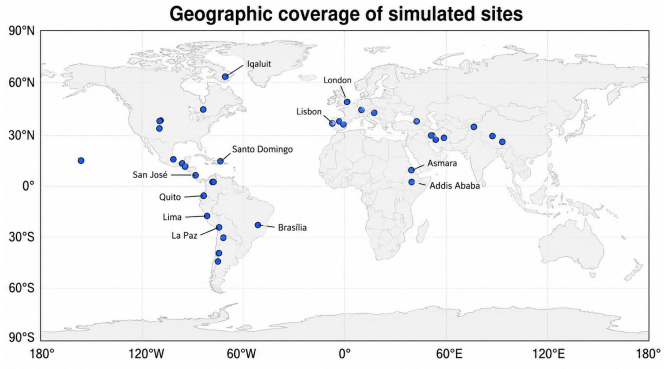

Deep learning flux generation and web deployment

We use CORSIKA outputs as training data, so the AI model can generate muon fluxes faster.

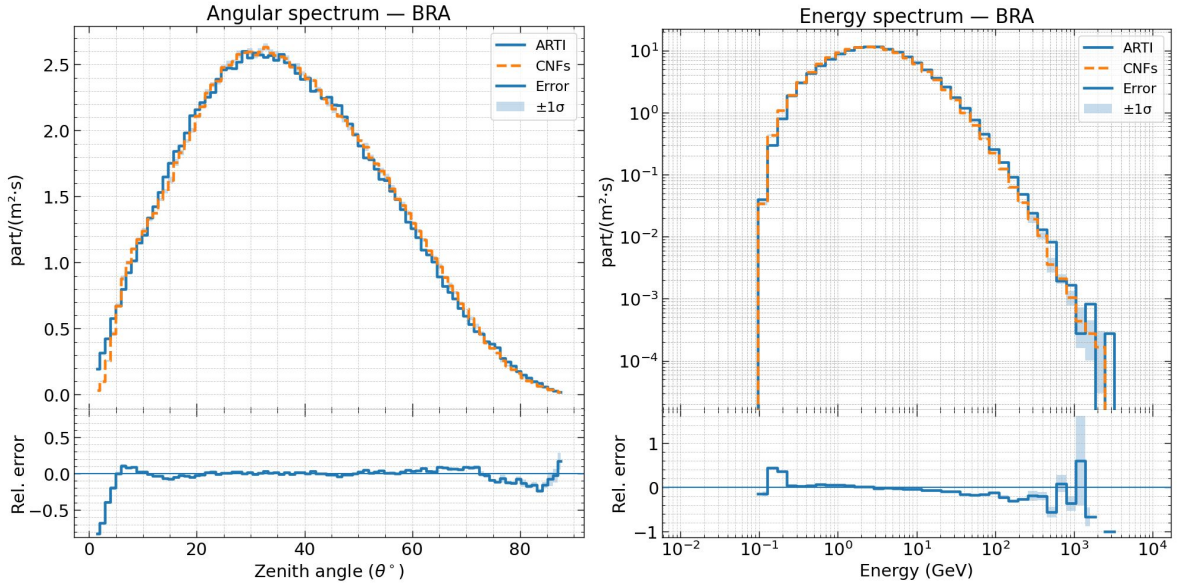

https://muon-generator.vercel.app/

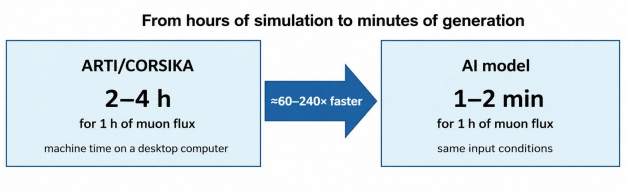

Warning: Web runs may take ~3–4 min in this pilot phase.

Now that we have the flux, we can propagate it through the volcano.

Backpropagation through the volcano

We convert detector directions into rock thickness, and then into a muon survival condition.

- Detector angles are traced through the volcano geometry.
- Each direction gives a rock thickness.
- CSDA converts rock thickness into a critical energy.
- Muons survive only if $E_\mu \geq E_{\mathrm{crit}}(L, \rho)$

Geometry Filtering → Ray Back propagation → CSDA → Energy condition

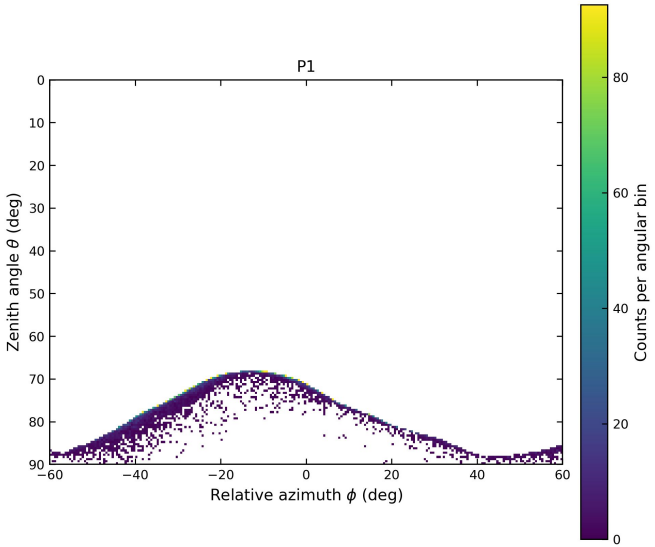

Now we know which muons survive. But they do not travel in perfect straight lines.

Backpropagation through the volcano

We convert detector directions into rock thickness, and then into a muon survival condition.

- Detector angles are traced through the volcano geometry.
- Each direction gives a rock thickness.
- CSDA converts rock thickness into a critical energy.
- Muons survive only if $E_\mu \geq E_{\mathrm{crit}}(L, \rho)$

Geometry Filtering → Ray Back propagation → CSDA → Energy condition

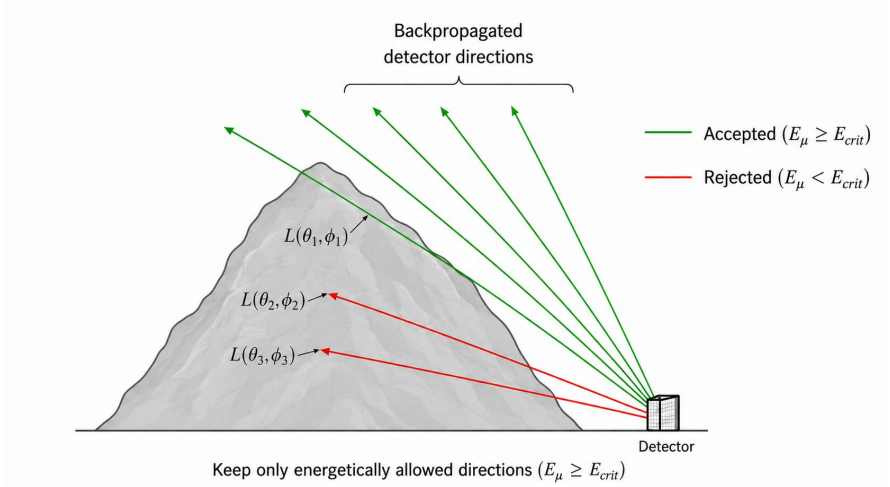

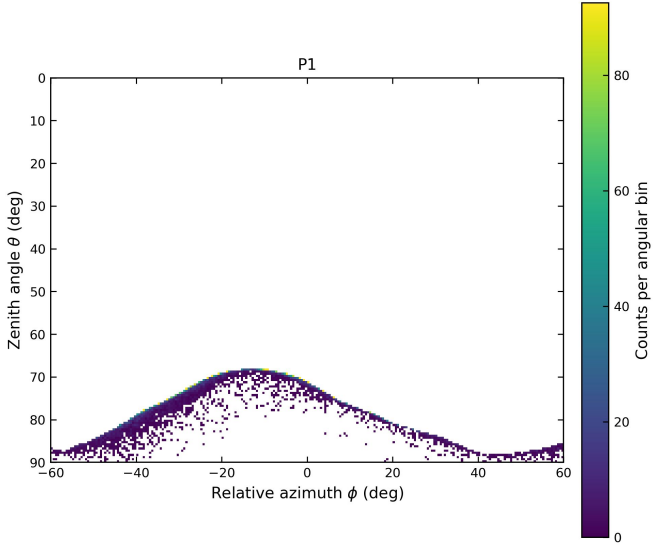

Now we know which muons survive. But they do not travel in perfect straight lines.

Why do we need a scattering kernel?

After the volcano filter, muons survive, but they do not travel in perfect straight lines.

- Straight-line propagation ignores angular scattering.
- Lynch & Dahl gives a first scattering scale.
- But it does not describe the full migration pattern.
- Geant4 gives detailed exit-angle distributions.
- These distributions are stored in an empirical kernel.

$$\theta_0 = \frac{13.6\ \text{MeV}}{\beta c p}\, z \sqrt{\frac{x}{X_0}} \left[1 + 0.088 \log_{10}\left(\frac{x\, z^2}{X_0 \beta^2}\right)\right]$$

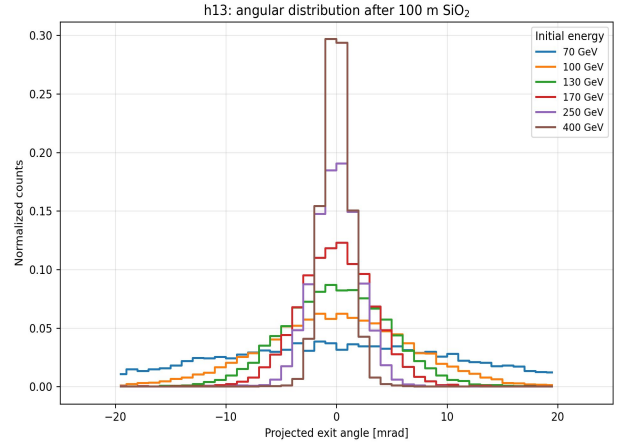

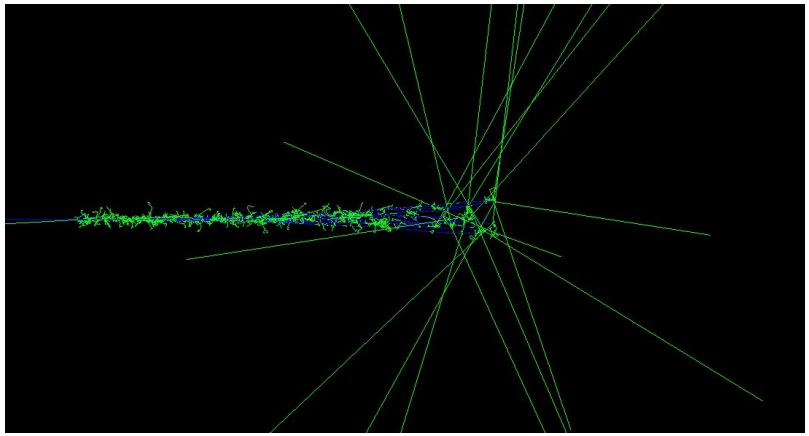

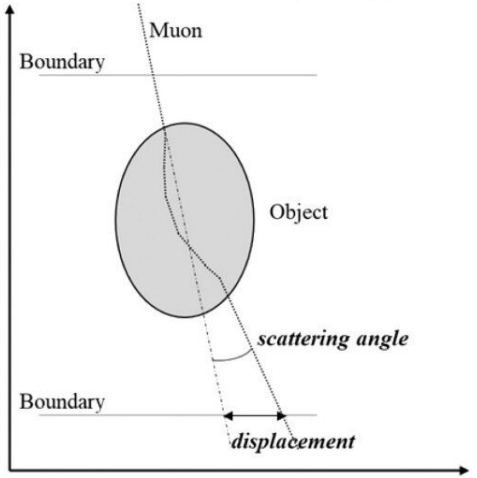

Highland, NIM 129, 497–499 (1975); Lynch & Dahl, NIM B 58, 6–10 (1991).

Scattering changes the final muogram

We run Geant4 once, and reuse the result many times.

- Run Geant4 for many thickness–energy cases.
- Store the exit-angle distributions.
- Convert them into probability kernels.
- Apply the kernel to surviving muons.
- Obtain the scattered muogram.

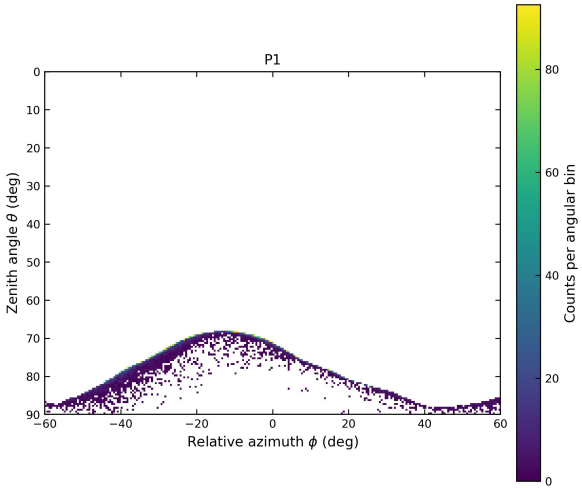

Lynch & Dahl

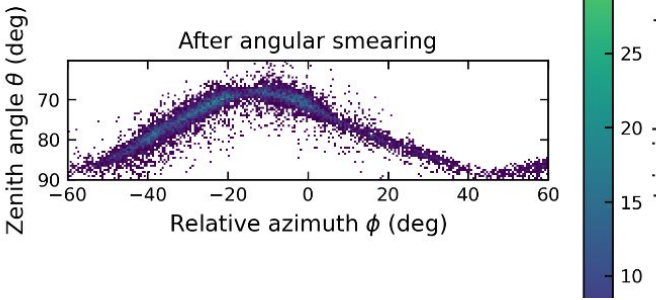

Our kernel

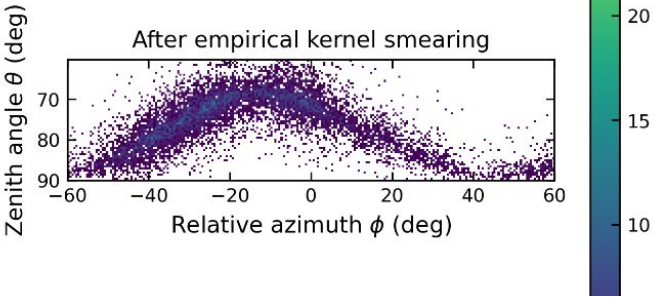

Next step: apply the model and compare it with real measurements.

MuTe: En una slide

- Barras centelleadoras plásticas con lectura por fibra óptica.
- SiPM Hamamatsu.
- Electrónica CAEN FERS A5202/DT5202 de 64 canales.
- Trigger configurable: OR, mayoría y coincidencias.
- Modo de operación: OR32_AND2 para eventos correlacionados.
- Monitoreo continuo de temperatura, humedad y presión.
- Operación remota en campo mediante Starlink.
- Sistema preparado para adquisición estable y prolongada.

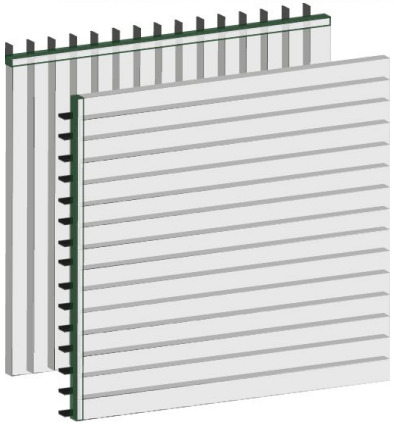

Real MuTe data for model comparison

We use the current mountain-facing campaign to compare the simulated shadow with measured muon data.

- Mountain-facing MuTe campaign from the laboratory building.
- More than 100 days of accumulated muon data.
- 4-fold coincidence events are used for the measured flux.
- Large rock thickness produces a strong open-sky flux suppression.

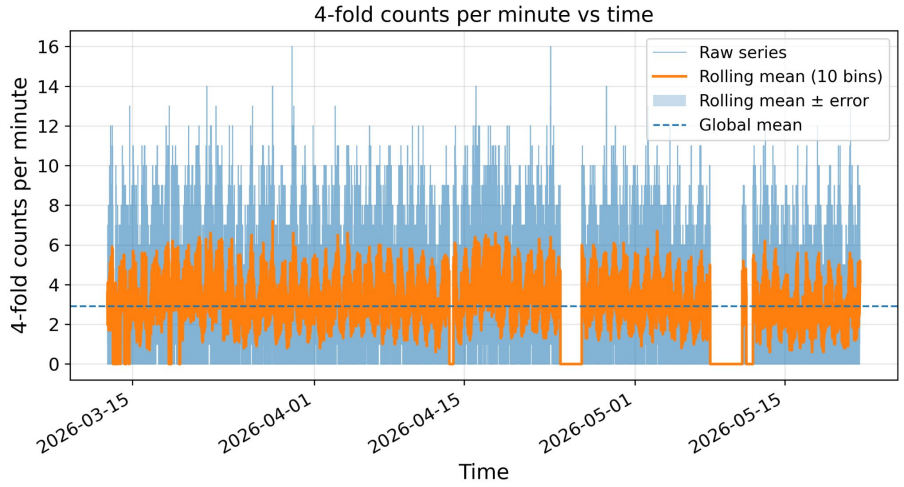

Muon shadow from the Andes: measurement and simulation

The measured mountain shadow is compared with the simulated muogram.

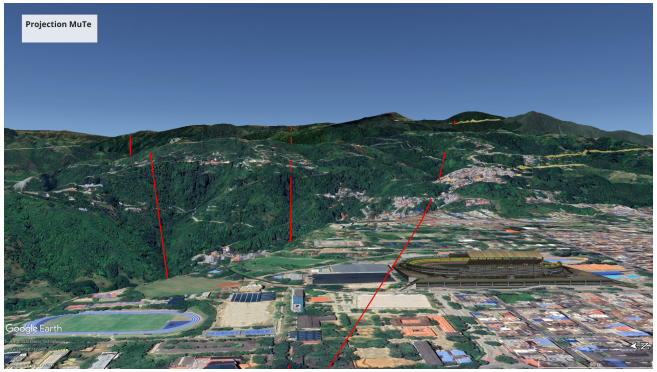

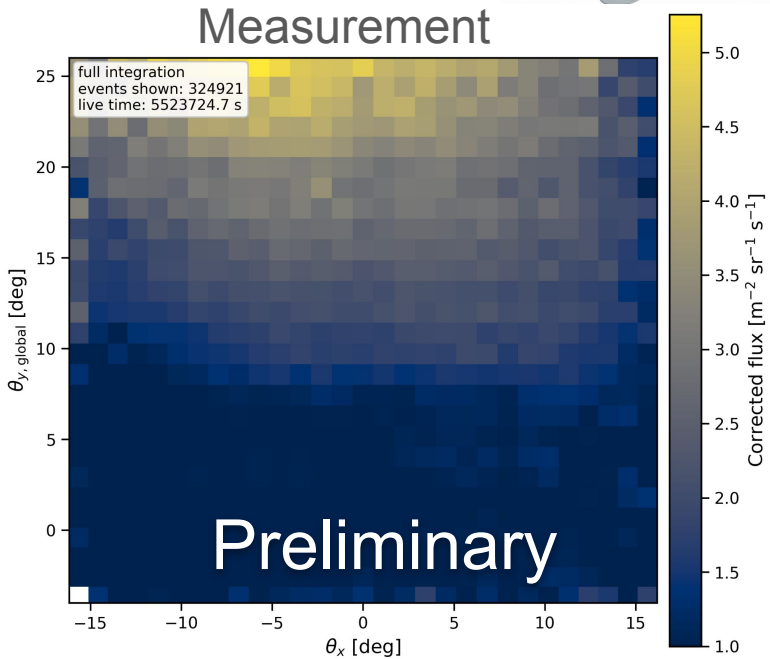

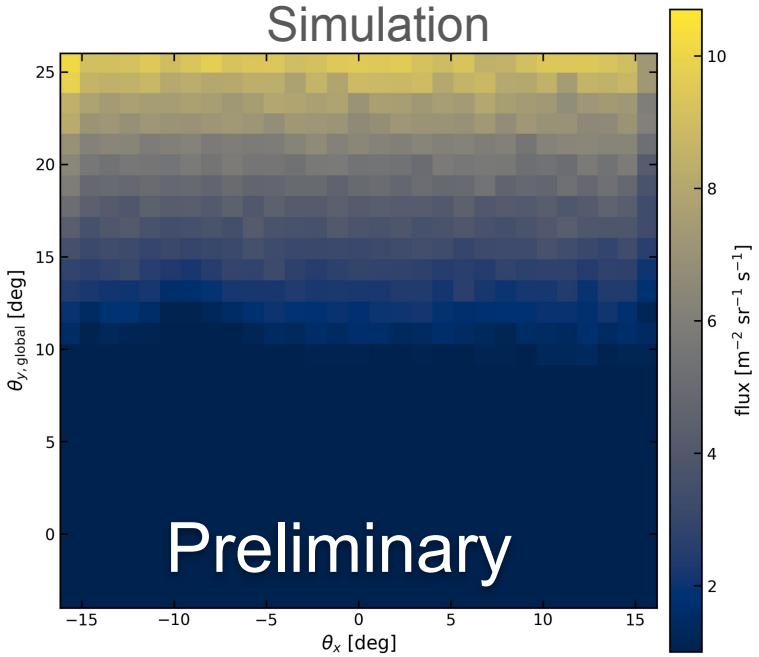

MuTe
The Muon Telescope

Universidad Industrial de Santander

CYTED

LAGO

LIDeRA

Gracias

Rafael A. Martínez Rivero.
rafael2248058@correo.uis.edu.co

Scattering changes the final muogram

We run Geant4 once, and reuse the result many times.

- Run Geant4 for many thickness–energy cases.
- Store the exit-angle distributions.
- Convert them into probability kernels.
- Apply the kernel to surviving muons.
- Obtain the scattered muogram.

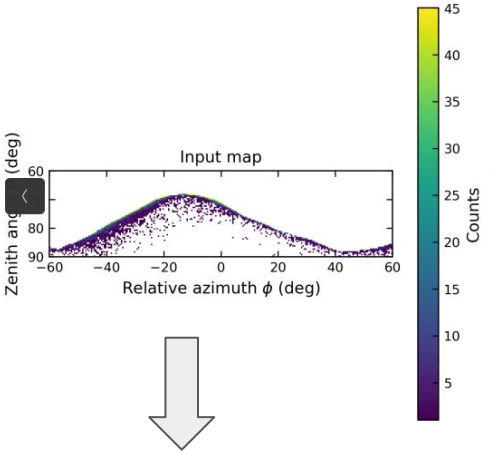

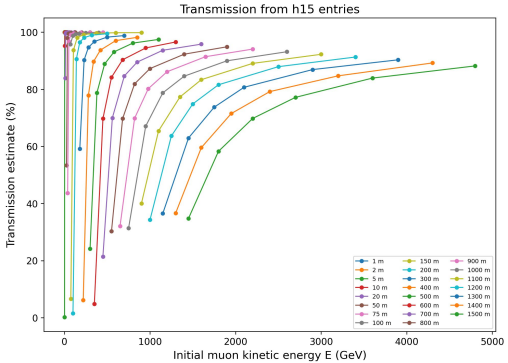

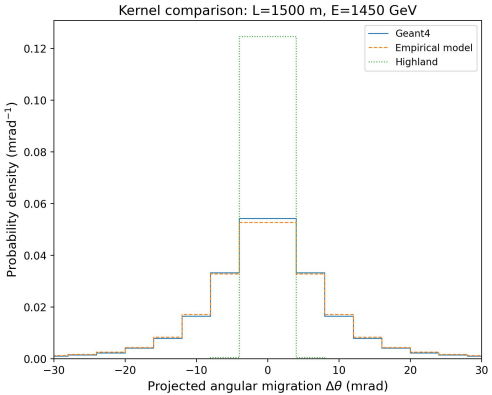

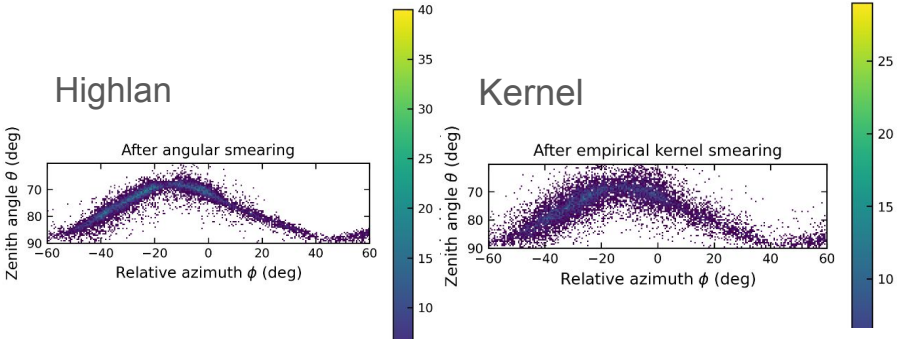

Next step: apply the model and compare it with real measurements.

ARTI-Model in energy bands

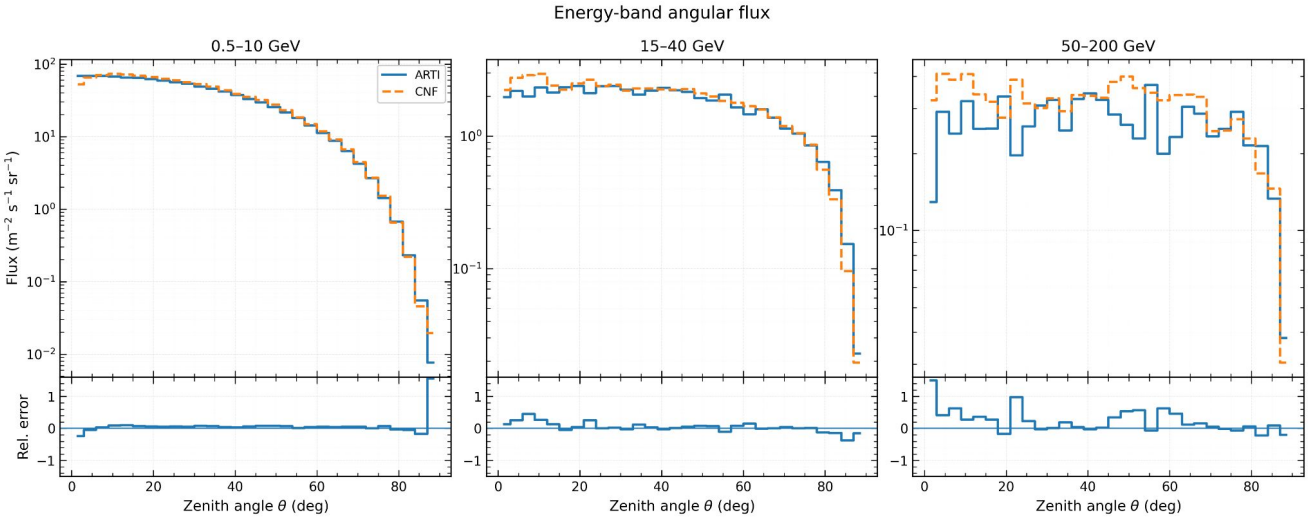

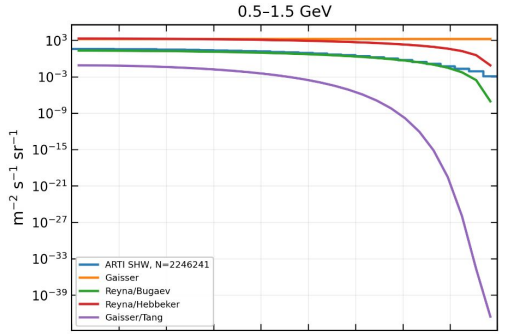

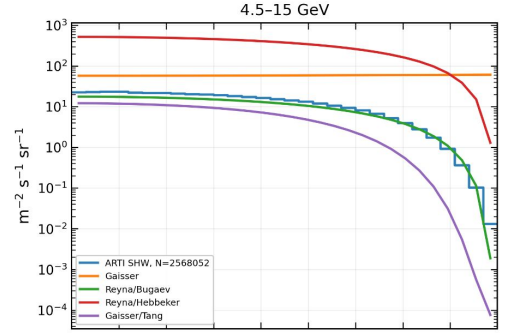

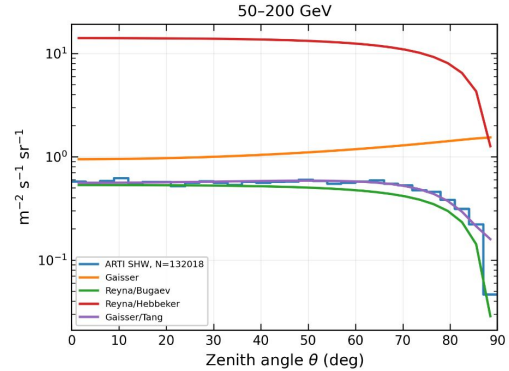

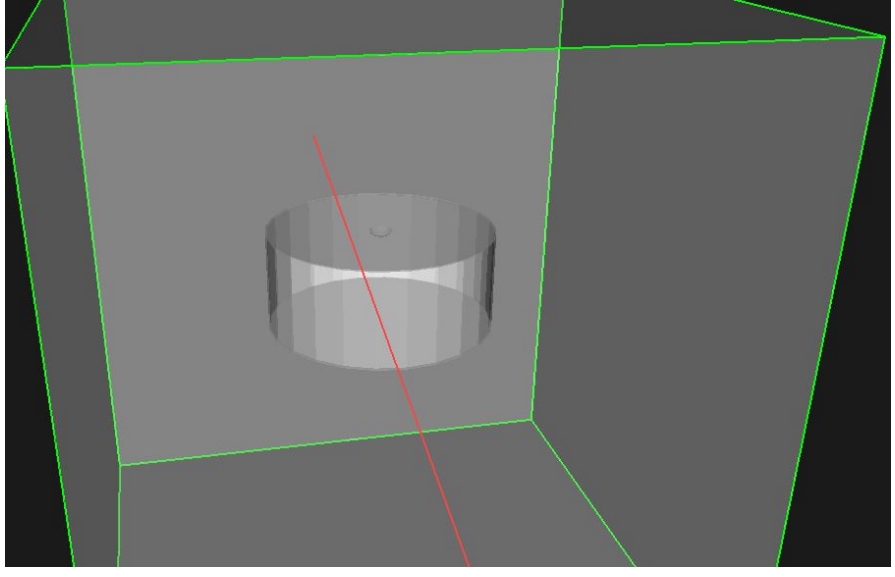

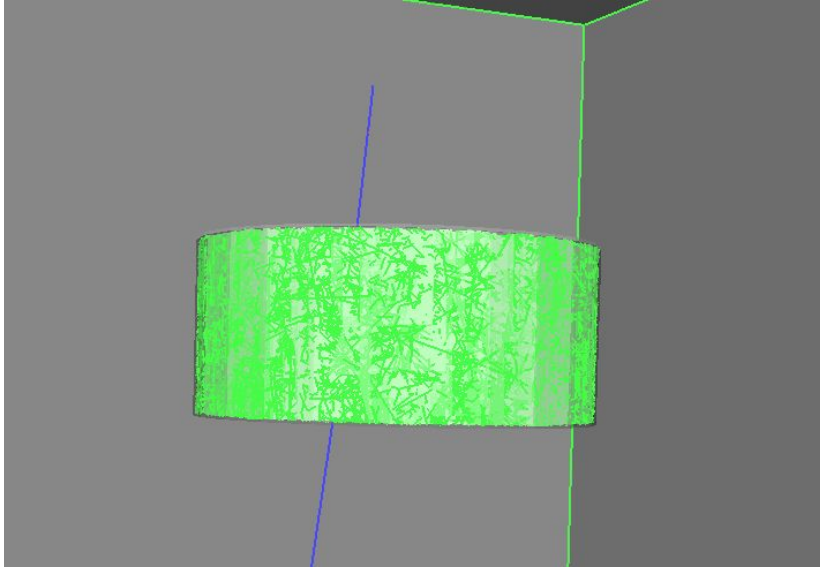

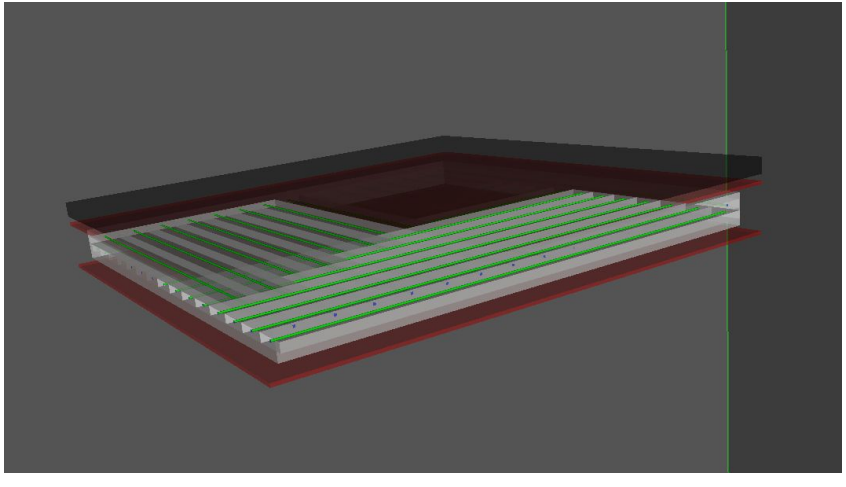

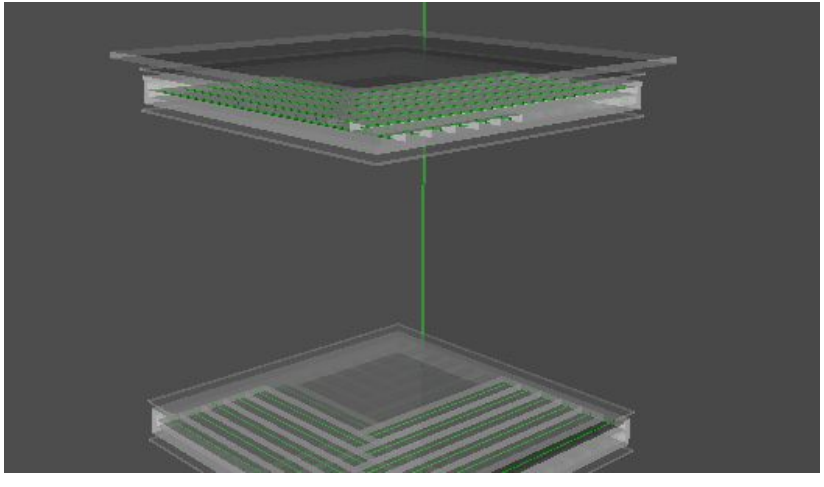

From Full MC to fast kernel of MCS: Muogram impact

$$K(\Delta\Omega|E_\mu,L,\rho)=p(\Omega_{\text{out}}-\Omega_{\text{in}}|E_\mu,L,\rho),\ \int K(\Delta\Omega|E_\mu,L,\rho)\,d(\Delta\Omega)=1.$$

$$N_{\text{scat}}(\Omega_{\text{rec}})=\int dE_\mu\,d\Omega\,N_{\text{surv}}(E_\mu,\Omega)\,K(\Omega_{\text{rec}}-\Omega|E_\mu,L(\Omega),\rho).$$

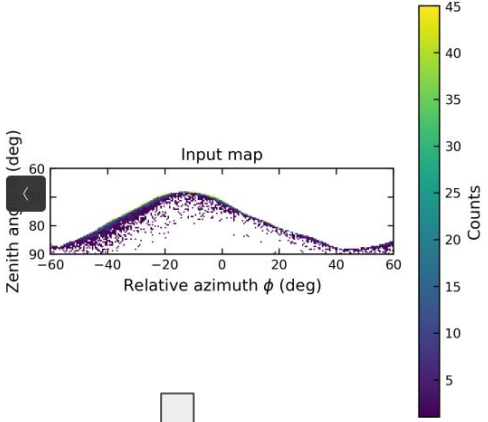

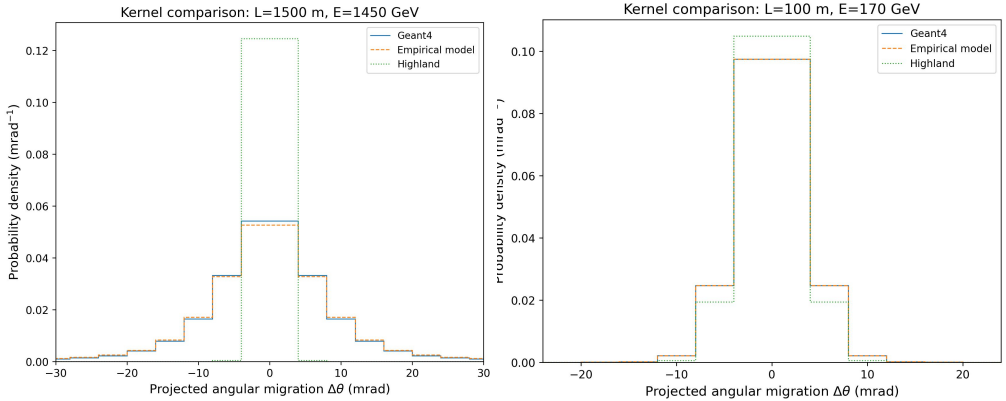

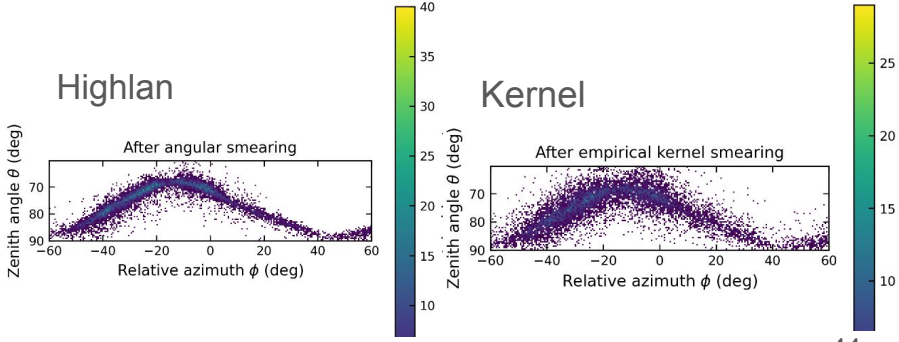

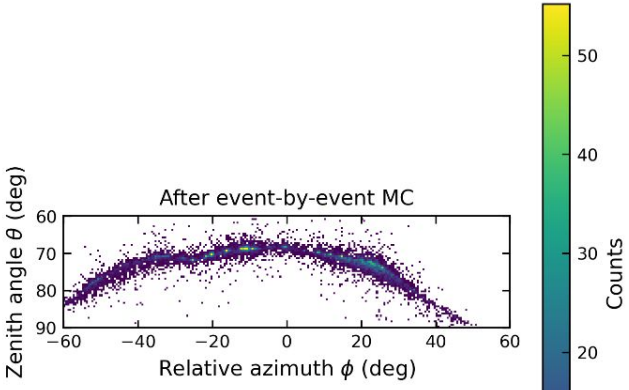
After event-by-event MC
Zenith angle θ (deg)
Relative azimuth ϕ (deg)
Counts

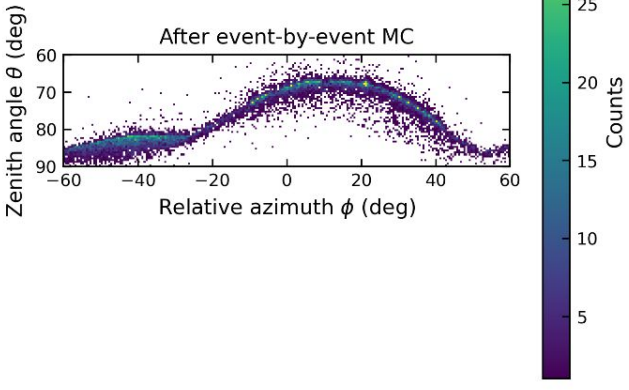
After event-by-event MC
Zenith angle θ (deg)
Relative azimuth ϕ (deg)
Counts

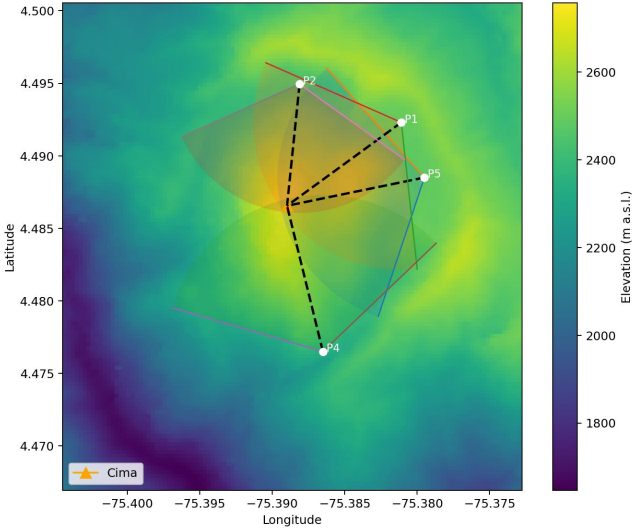
P1
P2
P4
P5
Cima
Latitude
Longitude
Elevation (m a.s.l.)

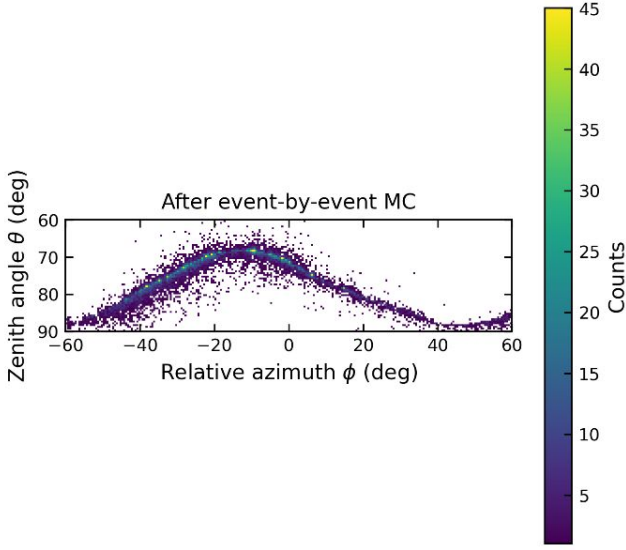
After event-by-event MC
Zenith angle θ (deg)
Relative azimuth ϕ (deg)
Counts

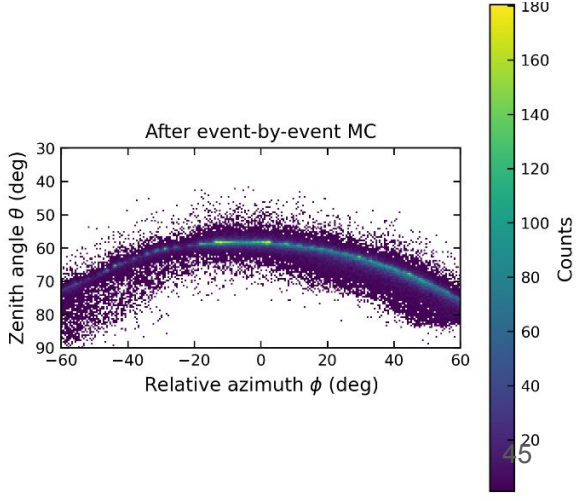
After event-by-event MC
Zenith angle θ (deg)
Relative azimuth ϕ (deg)
Counts

Geant4 Simulation

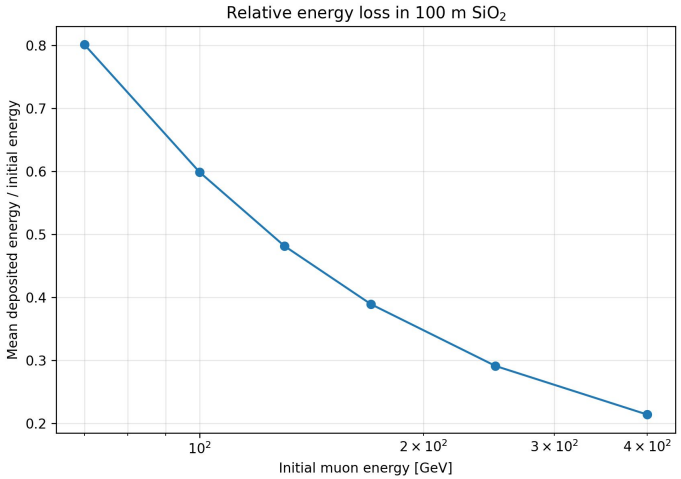
Relative energy loss in 100 m SiO_2
Mean deposited energy / initial energy
0.8
0.7
0.6
0.5
0.4
0.3
0.2
10^2
2×10^2
3×10^2
4×10^2
Initial muon energy [GeV]

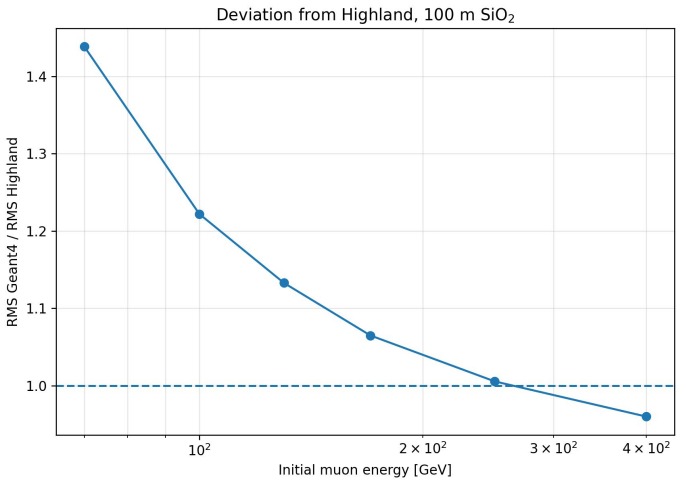
Deviation from Highland, 100 m SiO_2
RMS Geant4 / RMS Highland
1.4
1.3
1.2
1.1
1.0
10^2
2×10^2
3×10^2
4×10^2
Initial muon energy [GeV]

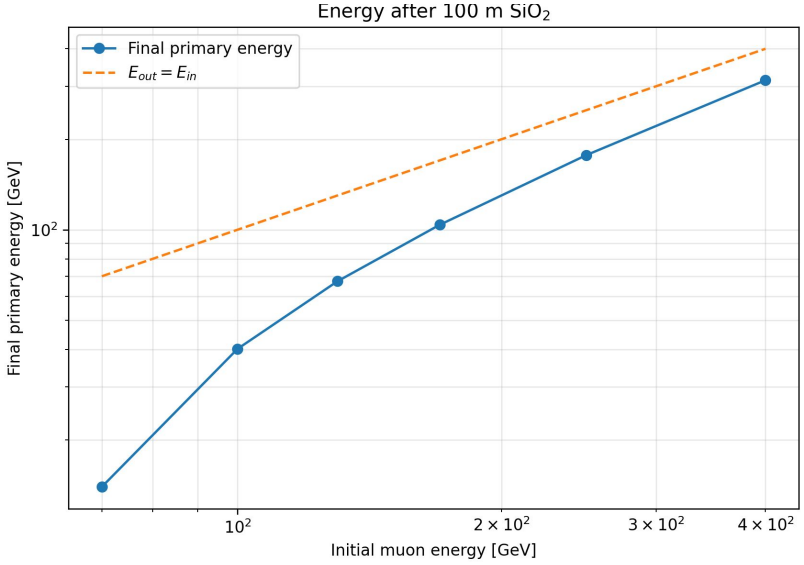
Energy after 100 m SiO_2
Final primary energy
$E_{out} = E_{in}$
Final primary energy [GeV]
10^2
10^2
2×10^2
3×10^2
4×10^2
Initial muon energy [GeV]

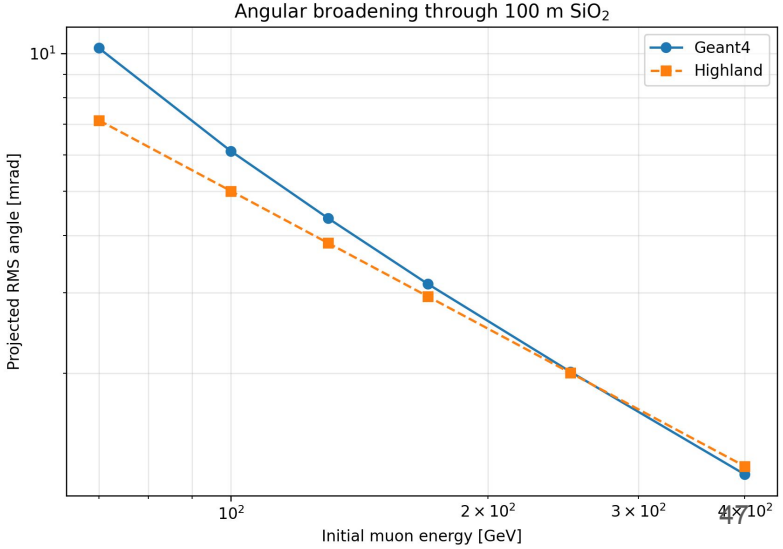
Angular broadening through 100 m SiO_2
Geant4
Highland
Projected RMS angle [mrad]
10^1
10^2
2×10^2
3×10^2
4×10^2
Initial muon energy [GeV]

Exit-angle distribution

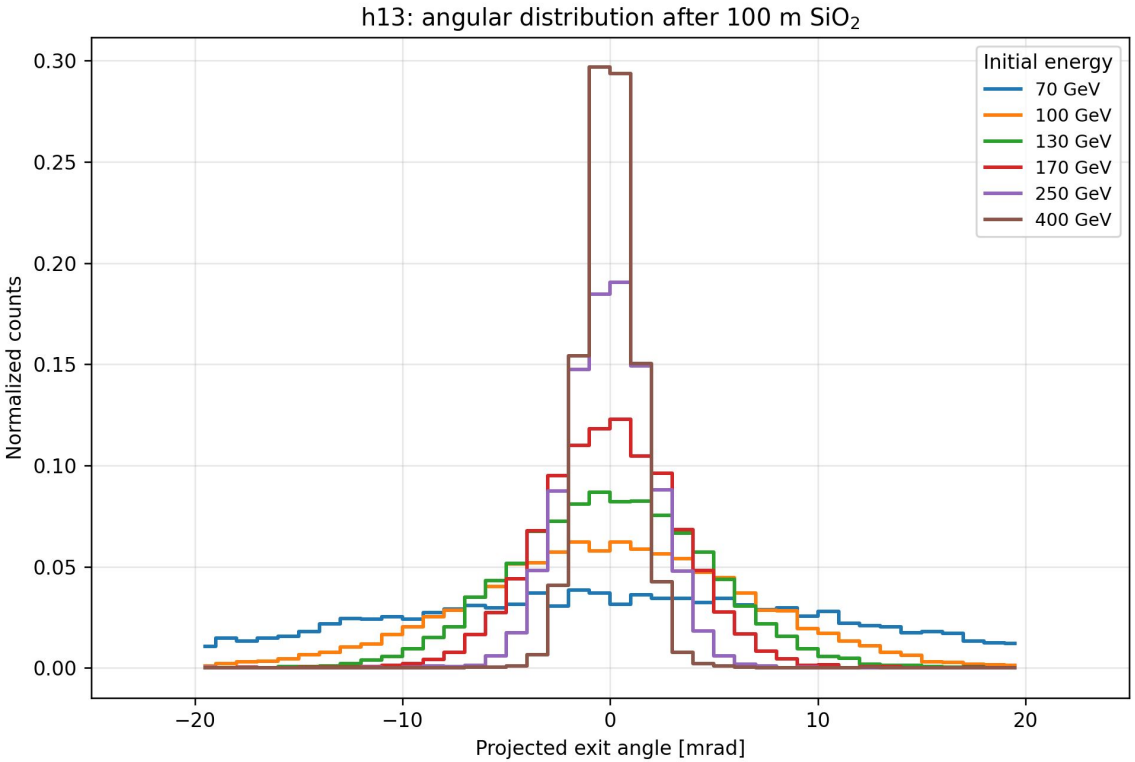

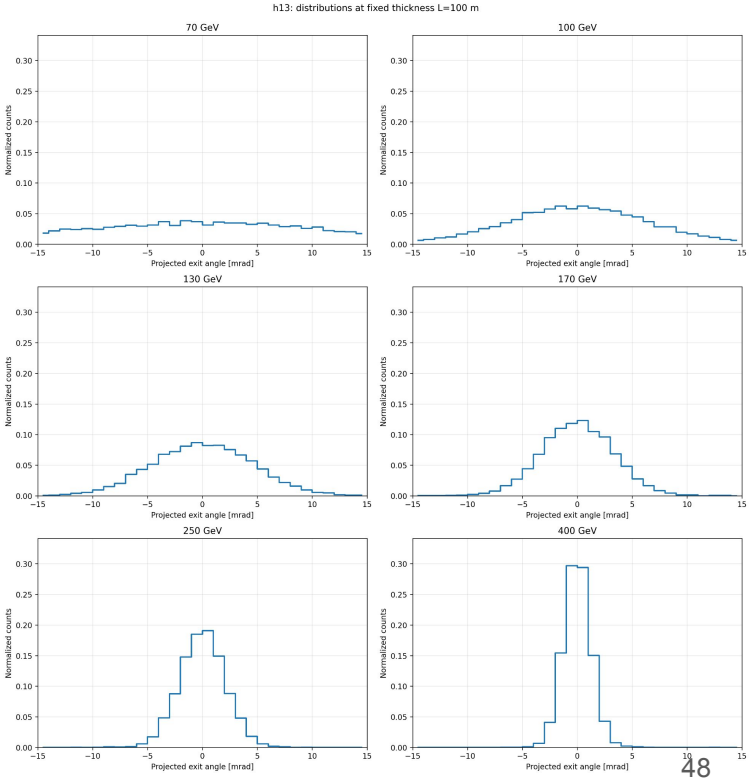

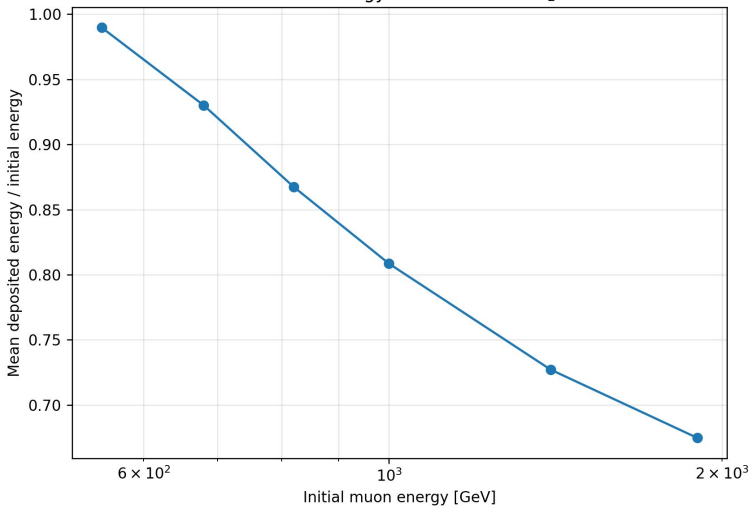
Relative energy loss in 800 m SiO_2
Mean deposited energy / initial energy
1.00
0.95
0.90
0.85
0.80
0.75
0.70
6×10^2
10^3
2×10^3
Initial muon energy [GeV]

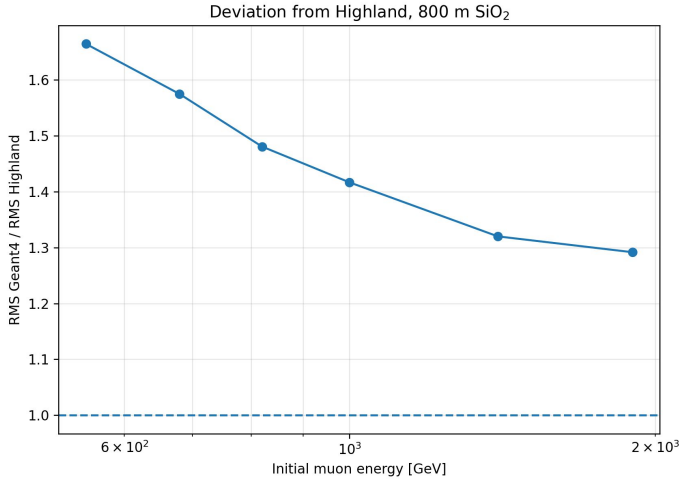
Deviation from Highland, 800 m SiO_2
RMS Geant4 / RMS Highland
1.6
1.5
1.4
1.3
1.2
1.1
1.0
6×10^2
10^3
2×10^3
Initial muon energy [GeV]

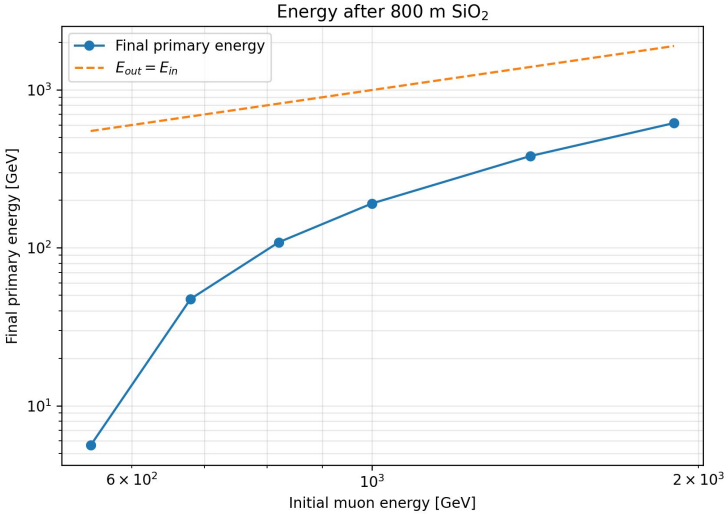
Energy after 800 m SiO_2
Final primary energy
$E_{out} = E_{in}$
Final primary energy [GeV]
10^3
10^2
10^1
6×10^2
10^3
2×10^3
Initial muon energy [GeV]

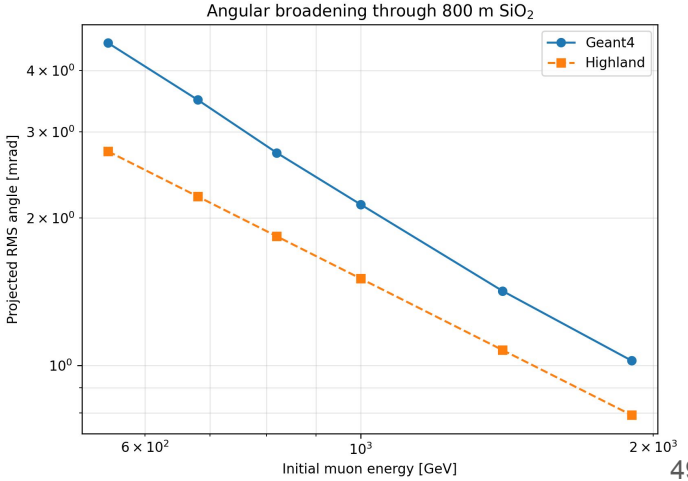
Angular broadening through 800 m SiO_2
Geant4
Highland
Projected RMS angle [mrad]
4×10^0
3×10^0
2×10^0
10^0
6×10^2
10^3
2×10^3
Initial muon energy [GeV]